Advanced Filler Network Characterization in Rubber

Von der Naturwissenschaftlichen Fakultät der
Gottfried Wilhelm Leibniz Universität Hannover

zur Erlangung des Grades
Doktor der Naturwissenschaften (Dr. rer. nat.)

genehmigte Dissertation
von

Syed Imran Hussain Syed Javaid Iqbal, M. Sc.

2021

Abstract

The present work is aimed at introducing new characterization techniques in filled rubber compounds. Rubber fillers such as carbon black are often used to enhance the physical properties of rubber compounds. With a sufficient amount of carbon black, a percolated filler network is formed, spanning the volume of the rubber compound. This phenomenon not only significantly improves the mechanical material behaviour, but also introduces a more complex mechanical response. Further enhancement is possible with the addition of reinforcing resins such as Novolaks, phenol–formaldehyde resins with a formaldehyde-to-phenol molar ratio of less than one. Based on the systematic studies performed, the two reinforcing materials are observed to exhibit synergistic behaviour resulting from their physical and chemical interaction.

The reinforcing resin modifies the activity of the filler surface creating a more compact filler network. This leads to a lower filler network percolation threshold as well as increasing the reinforcing behaviour. This conclusion was derived from various thermo-mechanical measurements such as temperature stress scanning relaxation (TSSR) and dynamic mechanical analysis (DMA). The findings were also validated with advanced microscopical techniques such as atomic force microscopy (AFM) and transmission electron microscopy (TEM).

A direct consequence of the filler network is a strain dependent behaviour such as the dynamic and quasi-static strain dependent softening effects known as Payne and Mullins effects, respectively. Within the conventional dynamic mechanical analysis (DMA) of rubber compounds, the mechanical response signal is often assumed to be rheologically linear (sinusoidal function) since in Fourier space, the first harmonic is more pronounced than the subsequent higher harmonics. However, valuable information contained in the higher harmonics can be utilised in order to further characterise the compound properties. One such approach is the large amplitude oscillatory shear (LAOS) technique which analyses the harmonics as a function of large strain deformation. While several studies have contributed to the understanding of this strain dependent nonlinearity, less emphasis was placed on the nonlinearity of the frequency domain. Utilising a resonance-based high frequency DMA, nonlinearities in the frequency domain were established by the observation of the superharmonic resonance, for the first time in rubber technology.

Two distinct nonlinearities were observed, polymer induced nonlinearity and filler induced nonlinearity. The new method based on the superharmonic resonance has been successfully applied to characterise the filler network through the evaluation of the microdispersion of carbon black and its interaction with reinforcing resins.

Keywords: Superharmonic resonance, HF DMA, filler network

i

Kurzzusammenfassung

Die vorliegende Arbeit hat das Ziel, innovative Methoden zur Charakterisierung von gefüllten Kautschukmischungen einzuführen. Füllstoffe, wie Ruß, werden in Kautschuk eingesetzt, um seine physikalischen Eigenschaften zu verstärken. Mit einer ausreichenden Menge an Ruß wird ein perkolierendes Netzwerk erzeugt, das das Volumen der Kautschukmischung durchdringt. Diese Erscheinung verstärkt nicht nur das mechanische Materialverhalten, sondern führt zu einer komplexeren mechanischen Reaktion. Eine weitere Verstärkung ist durch den Einsatz netzwerkbildender Harze möglich, z.B. von Novolaken, Phenolharzen mit einem Formaldehyd-Phenol-Verhältnis kleiner eins. Auf der Basis von systematischen Studien wird ein synergistisches Verhalten der beiden verstärkenden Materialien infolge ihrer physikalischen und chemischen Wechselwirkung beobachtet.

Das Verstärkungsharz verändert die Aktivität der Füllstoffoberfläche und erzeugt damit ein kompakteres Füllstoffnetzwerk. Dies führt zu einer reduzierten Perkolationsschwelle sowie zu einer zusätzlich höheren Verstärkung. Diese Schlussfolgerung wurde aus Messungen mit verschiedenen thermomechanischen Verfahren abgeleitet, wie der anisothermen Spannungsrelaxation (TSSR) und der dynamisch-mechanischen Analyse (DMA). Die Ergebnisse wurden auch mit anspruchsvollen mikroskopischen Techniken validiert, wie der Rasterkraftmikroskopie (AFM) und Transmissionselektronenmikroskopie (TEM).

Eine direkte Folge des Füllstoffnetzwerks ist die Entstehung eines dehnungsabhängigen Verhaltens, das als dynamischer oder quasi-statischer Erweichungseffekt beobachtet und jeweils als Payne- oder Mullins-Effekt bezeichnet wird. Bei der dynamisch-mechanischen Analyse (DMA) von Kautschukmischungen wird häufig eine Linearität der Antwort in Bezug auf das angelegte Verformungssignal angenommen, da die Stärke der ersten Harmonischen viel höher ist als die der nachfolgenden Harmonischen. Es gibt jedoch wertvolle Informationen in den höheren Harmonischen, die verwendet werden könnten, um die Materialeigenschaften weiter zu charakterisieren. Ein solcher Ansatz ist die LAOS-Technik (engl. Large Amplitude Oscillatory Shear), mit der die Harmonischen als Funktion der Dehnung analysiert werden. Während einige Studien bereits zum Verständnis dieses dehnungsabhängigen Phänomens beigetragen haben, wurde weniger Wert auf die Nichtlinearität im Frequenzbereich gelegt. Unter Verwendung einer resonanzbasierten Hochfrequenz-DMA wurden erstmals in der Kautschuktechnologie Nichtlinearitäten im Frequenzraum durch Beobachtung von superharmonischen Resonanzen festgestellt.

Zwei unterschiedliche Typen von Nichtlinearitäten wurden beobachtet, die polymerinduzierte und die füllstoffinduzierte Nichtlinearität. Die neue Methode auf der Basis der superharmonischen Resonanz wurde zur Charakterisierung des Füllstoffnetzwerkes durch Bewertung der Mikrodispersion von Ruß und dessen Wechselwirkung mit verstärkenden Harzen erfolgreich eingesetzt.

Keywords: Superharmonische Resonanz, HF DMA, Füllstoffnetzwerk

Acknowledgements

Contents

List of Figures

Chapter 1

Introduction

1.1 General Introduction

Cured rubber was invented by both Charles Goodyear and Thomas Hancock in 1840s [1], marked the first time at which raw rubber products are able to withstand high mechanical load while retaining its elasticity. This was done through a process known as vulcanization whereby a mixture of raw rubber material and sulfur is heated to form chemical crosslinks within the rubber compound. These chemical crosslinks could also be introduced via peroxide-based vulcanization.

In the early 18th century, most rubber based products were made from natural rubber, most of which originated from the rubber tree *Hevea Brasiliensis*. The latex produced from these trees were composed of polyisoprene with a very high (>99%) content of 1,4-cis-isomer [2]. The quality of raw natural rubber such as polymer chain length and inorganic contents, varies with respect to the climate and soil.

Driven by the demands of the automobile industry, the first synthetic rubber was invented by Fritz Hofmann in 1909. This invention would play a large role in the subsequent decades as war led to severe shortages of natural resource. In the 1930s, Walter Bock had invented Styrene-Butadiene Rubber (SBR or formerly known as Buna-S) which was meant as a replacement for natural rubber [3]. All synthetic rubber however is not as mechanically durable as natural rubber and therefore natural rubber remains an important ingredient in the industry.

Fast forward to the present day, rubber remains one of the predominant material in our daily lives. Its wide range of applications includes tires, seals, hoses, electrical insulators and many more. It is a class of material that is able to deform and retain its original shape after the force is unloaded. There are various ways of modifying this property, one of which is the addition of reinforcing fillers.

The most common example of reinforcing fillers are carbon blacks. Chemically made of more than 95% of elemental carbon, they are produced by either thermal-oxidative decomposition or thermal decomposition [4, 5]. The former is the most widely used process due to the high production output and could generate a wide range of carbon black grades by water quenching. When a rubber matrix

is coupled with reinforcing fillers, a significant mechanical improvement are made with respect to elongation at break, stiffness, abrasion and others [5]. In addition, these properties can be further enhanced by the use of reinforcing resins [6].

One key feature of filled rubber compound is the nonlinear mechanical response to large deformations. This is a non-trivial matter as it infers that the mechanical processes involved are operating at a certain frequency and temperature ranges. While it is known from rheological studies in Fourier space, that fillers induce nonlinearity within the large amplitude of deformation [7], little is known within the frequency response of the material. Thus, an investigation of the mechanical nonlinear response for rubber compounds is presented here. Within the scope of this dissertation, we limit ourselves to the investigation of rubber nonlinearity at relatively high frequencies, within kilohertz's range and under ambient conditions.

1.2 Experimental Approach

In the present work, various experimental methods were performed in order to characterise the mechanical impact of fillers in rubber compounds. Three broad experimental approaches were used; microscopic techniques, quasi-static thermo-mechanical deformation and dynamic mechanical measurements. The latter two are the main focus in this dissertation.

The recently approved standard ASTM D8363 Stress Relaxation in Tension Under Non-Isothermal Conditions, also known as Temperature Scanning Stress Relaxation (TSSR) [8], is the main focus for the quasi-static thermo-mechanical experiment as it was used to investigate the rate of stress decay on the resin reinforced filler network. The basis of this experimental setup is the measurement of the stress relaxation of a pre-stretched sample, undergoing a defined temperature ramp. The outcome is the relaxation spectrum which can be decomposed to different relaxations processes due to polymer and filler network properties.

A novel approach in material characterization is presented by analysing the vibrational response of rubber compounds. The VHF104 by Metravib, Lyon, France is able to measure a dynamic mechanical response up to 10 kHz by utilizing the resonance of the material. Within Fourier space, a superharmonic resonance phenomenon is observed which has not been discussed elsewhere in the field of rubber science. The superharmonic resonance can also be modelled in real space with a nonlinear Kelvin-Voigt viscoelastic model. In the present investigation, the Duffing oscillator model was used with cubic nonlinear term α in the elastic component [9].

1.3 Thesis Structure

The present work is arranged as a cumulative dissertation at which three peer-reviewed publications are compiled on the basis of the aforementioned title, "Advanced Filler Network Characterization in Rubber". In the subsequent second chapter, a quick revision on several rubber science concepts are

presented which serve as a foundation for the thesis. This is followed by the methodology chapter, whereby the experimental setup is described. In chapter four, all three peer-reviewed publications are compiled with a short intermediary. In the final chapter, a summary of the current findings are explicitly stated as well as the a future outlook of the topic.

Chapter 2

Literature Review

2.1 Rubber
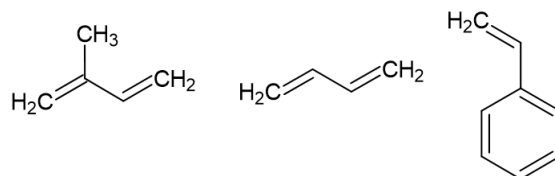
FIGURE 2.1: Three of the most commonly used monomers in rubber today; isoprene (left), butadiene (middle) and styrene (right).

First proposed by Hermann Staundinger in the 1920s [10], polymers are macromolecules that are compose of smaller identical molecular sub-units, called monomers. Polymers can exist in either semi-crystalline state or amorphous state. Apart from polymers with a high degree of crystallinity, all polymers are able exhibit the glass transition temperature, Tg. On the molecular level, it is the temperature at which large segmental motions of polymer chains are observed within the time scale of the experiment [11]. Polymers with Tg lower than room temperature are called rubber [12].

The biggest consumer of rubber is the tire industry[13]. The four main general purpose elastomers are natural rubber (NR), polyisoprene (IR), polybutadiene (BR) and Styrene-Butadiene (SBR) rubber. The corresponding monomers are shown in figure 2.1. Note that even though NR and IR and chemically similar, but their tacticity and molecular weight differs significantly. NR is a form of bio-polymer and it typically has a molecular weight between 10^4 - 10^6 g/mol [14] with a high degree of either cis-1,4-polyisoprene or trans-1,4-polyisoprene [15]. This is mainly attributed to the polymerization process [16, 17]. Synthetic IR however is often polymerised with the Ziegler-Natta catalyst and has a lower molecular weight.

In material science, modulus ($= \frac{stress,\ \sigma}{strain,\ \varepsilon}$) is used to refer to the intrinsic stiffness of a material. Several common material modulus is summarised in table 2.1 and can be typically interrelated with the poisson's ratio ν, which is the ratio of transverse and longitudinal strains in tension [12]. Note
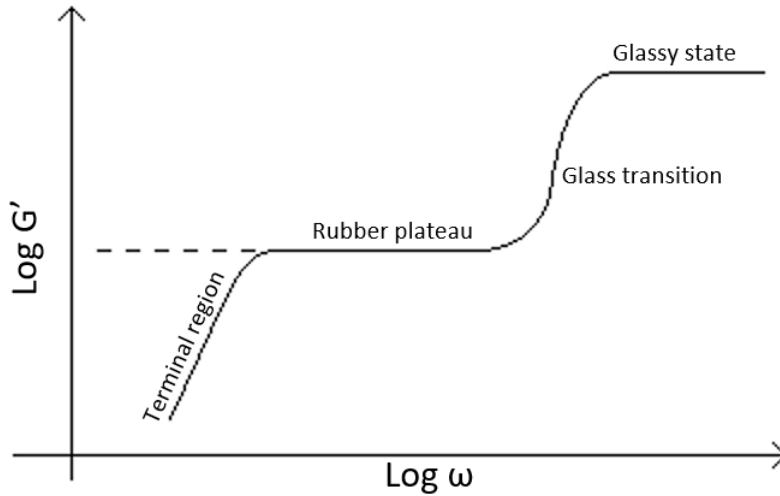
FIGURE 2.2: Master curve schematics for amorphous polymer materials. The dashed line indicates a crosslinked material.

TABLE 2.1: Modulus definition commonly used in material science

Symbol	Deformation mode
Young's modulus, E	Uniaxial extension
Shear modulus, G	Shearing mode
Bulk modulus, K	Compression
Longitudinal modulus, L	Wave propagation

that for incompressible material such as rubber, $\nu = 0.5$. For visco-elastic material, the modulus can be separated into two parts; real and imaginary:

$$M^* = M' + iM" \qquad (2.1)$$

The real part is termed as the storage modulus and is related to the elastic property of the material, while the imaginary part is termed as the loss modulus, representing the damping magnitude of the material. The ratio of loss to storage modulus is defined and the loss tangent:

$$tan\ \phi = \frac{M"}{M'} \qquad (2.2)$$

Further explanation of these parameters are presented in section 2.4 and 2.5.

One method of representing the visco-elastic behaviour of rubber is the so-called master curve as shown in figure 2.2. Based on the time-temperature superposition (TTS) principle, the applied frequency ω axis is inversely proportional to the applied temperature onto the material. At very high frequencies, the material is said to be in a glassy state as the polymer chains are immobile. At the rubber plateau, the high mobility of the polymer chains enables the amorphous polymer material to deform over relatively large strain. For polymer melts, the terminal region is visible since the polymer chains are able to slide with each other and henceforth, a diminishing mechanical

response can be observed [18]. This region is absent in a crosslinked rubber material as the polymer chains are chemically bonded with each other.

The rubber plateau modulus is a function of both entanglement density, the polymer chain length between two physically restricted points, and the crosslink density, the polymer chain length between two chemically restricted points [12]. In addition to the polymer chain modification, fillers could be added to further improve the mechanical properties of rubber material.

2.2   Fillers

There are two kinds of rubber fillers; reinforcing and non-reinforcing fillers. Fillers that does not significantly contribute to the mechanical properties of rubber are called non-reinforcing fillers. They are typically used to reduce the manufacturing cost of the final product by increasing its volume, reduce the stickiness behaviour and for pigmentation. Reinforcing fillers on the other hand, are able to create a network by clustering the filler-filler aggregates, and thus, significantly improve the mechanical properties of rubber. The three scales of filler morphology are shown in figure 2.3: primary particles, aggregates and agglomerates.
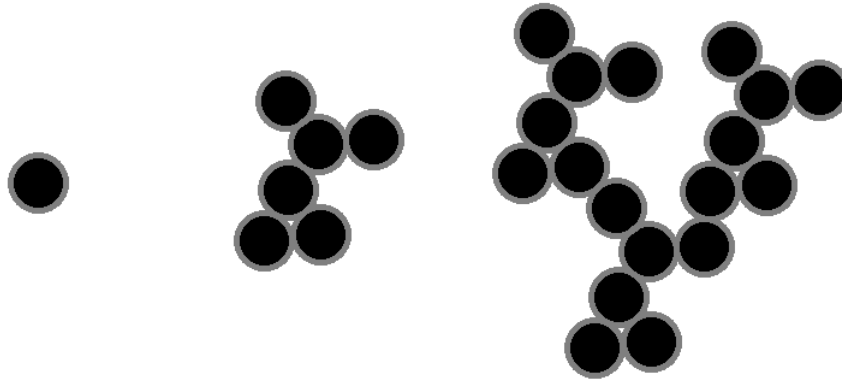
FIGURE 2.3: Filler morphology indicating primary particles (left), aggregates (middle) and agglomerates (right).

The primary particles are the smallest unit of filler morphology that constitutes the primary aggregates [4]. The degree of branching within the primary aggregates represents the filler structure, the first of two important filler morphology properties. The second filler property is the filler surface area. These properties dictate the interaction magnitude between the rubber and filler component. The primary aggregates are then clustered to form agglomerates.

The volume fraction of filler needed to obtain a filler network (i.e. filler agglomerates spanning the whole system) is defined as the filler percolation threshold ϕ_c. Hence, the mechanical behaviour of filled rubber can be generally separated into two regions, below the percolation threshold $\phi < \phi_c$ and above percolation threshold $\phi > \phi_c$. In the former case, the rubber is mechanical reinforced by hydrodynamics effects imposed by the isolated filler aggregates. The hydrodynamic effect concept

was introduced by Einstein with his work on fluid viscosity with dispersed rigid particle. In rubber science, the Einstein-Guth-Smallwood equation is often used to describe the mechanical behaviour under low deformation [19]:

$$G'(\phi) = G'_{unfilled}(1 + 2.5\phi + 14.1\phi^2),$$ (2.3)

where G' is the storage shear modulus, $G'_{unfilled}$ is the storage shear modulus without fillers and ϕ is the filler volume fraction.

Above ϕ_c, the filler network plays a dominant role in the mechanical properties of rubber. Essentially, the mechanical load applied on the rubber is directly transmitted through the filler network. Based on the Cluster-Cluster Aggregation (CCA) concept introduced by Klüppel and Heinrich, a universal scaling behaviour can be obtained by the fractal dimension of the filler aggregates [20].

The addition of filler in rubber introduces a strain-dependent mechanical response. There are two important phenomena related to this: the Payne and Mullins effect. Named after the British scientist A. R. Payne for his investigation in carbon black filled rubber, a strain dependency was observed in rubber samples under cyclic deformation within small strains. The drop in storage modulus corresponds to the break down of filler network and is often assumed to be fully reversible. The strain-dependent measurement of storage modulus can be separated into two regimes, the linear visco-elastic (LVE) and the nonlinear visco-elastic (NVE) region [7]. Figure 2.4 illustrate the different components contributing to the Payne effect. Mullins effect is similar to the Payne effect with the exception that it occurs in a quasi-static deformation with large strains. In contrast to the Payne effect, the Mullins effect is irreversible [21].
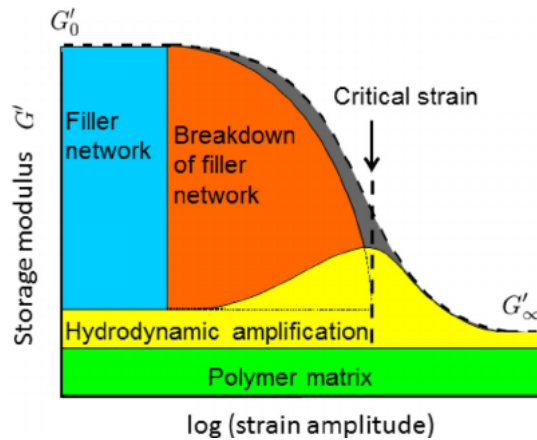
FIGURE 2.4: The Payne effect. [22]

2.3   Reinforcing Resins

Further mechanical improvements of a rubber compound can be made with the addition of reinforcing resin. Reinforcing resins are phenol-based chemical which is able to create a three dimensional resin

network with the aid of a methylene donor such as formaldehyde. The resin structure is a function of catalyst used, the ratio of phenol and formaldehyde, and the synthesizing temperature [23–26]. A common reinforcing resin reaction used in the tire industry is shown in figure 2.5. Consequently, the reinforcing resins improves the hardness of the compound as well as improve the compound mixing processibility since it acts as a softener prior to the curing step.
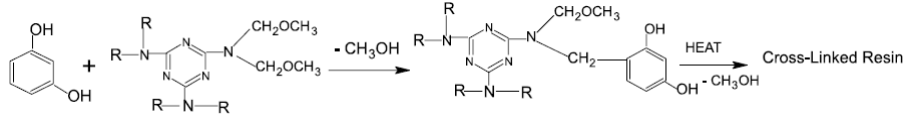
FIGURE 2.5: Reaction of diphenol and amine. [26]

In rubber compounds, the presence of hydroxyl groups leads to the reinforcing resins to be more polar than the rubber matrix. The difference in polarity would thus generate a binary-phase system at which the resins are immiscible with the rubber matrix [27]. The presence of carbon black improves the homogeneity of the compound by adhering the resin onto its surface. The combination of resin and carbon black thus leads to the lowering of the percolation threshold for the filler network. Hence, a synergistic effect between the two components [28, 29].

2.4   Mechanical Relaxation in Polymers

There are two fundamental relations used to describe the Hookean and the Newtonian flow behaviour:

$$\sigma = E\varepsilon \ , \tag{2.4}$$

where σ is the applied linear stress, E is the Young's modulus and ε is the strain.

$$\sigma_{shear} = \eta\dot{\gamma} \ , \tag{2.5}$$

where σ_{shear} is the applied shearing stress, η is the shear viscosity and $\dot{\gamma}$ is the shear rate.

It should be noted that equation 2.4 is similar to the equation 2.6 with the exception that the latter is often used to describe a shearing experiment while the former is used for uni-axial deformations.

$$\sigma_{shear} = G\gamma \tag{2.6}$$

The mechanical relaxation can be separated into two categories, under quasi-static and dynamic conditions.

2.4.1 Quasi-static deformation

An instantaneous application of either stress or strain can be defined by the quantity e_o describes the relaxation and retardation of visco-elastic systems.

$$e_o(t) = \begin{cases} 0 & for\ t < 0 \\ 1 & for\ t > 0 \end{cases} \tag{2.7}$$
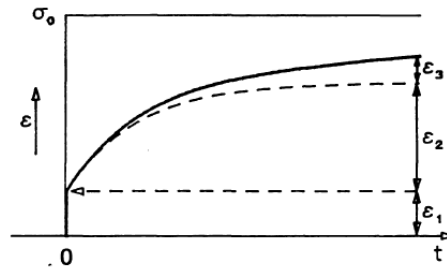
FIGURE 2.6: The three retardation components of creeping. [30]

Hence, in a quasi-static system of an instantaneous applied stress σ_o to a sample, the stress $\sigma(t)$ is defined as follows:

$$\sigma(t) = \sigma_o e_o(t), \tag{2.8}$$

In the time-dependent strain variable $\varepsilon(t)$, the applied stress thus induces a time-dependent creep:

$$\varepsilon(t) = \frac{1}{M(t)}\sigma_o = J(t)\sigma_o, \tag{2.9}$$

Where the compliance $J(t)$ is the reciprocal of the modulus M(t).

There are three main regions within the creeping response of material under deformation as shown in figure 2.6.

$$\varepsilon_1 = J_o\sigma_o \tag{2.10}$$

$$\varepsilon_2 = \sum_k \Delta J_k (1 - e^{(-\frac{t}{\tau_{\varepsilon k}})})\sigma_o \tag{2.11}$$

$$\varepsilon_3 = \frac{t}{\eta}\sigma_o \tag{2.12}$$

The three creep elements are strain Hookean deformation, "Highly elastic" deformation and Newtonian flow as designated by ε_1, ε_2 and ε_3 respectively. The highly deformation region is composed of a spectrum of relaxation times $\tau_{\varepsilon k}$. This discrete retardation spectrum can be replaced by a continuous retardation spectrum $L(ln\ \tau)$ [30, 31]:

$$J(t) = J_o + \int_{-\infty}^{\infty} L(ln\ \tau)(1 - e^{-\frac{t}{\tau}})d\ ln\ \tau + \frac{t}{\eta} \tag{2.13}$$

Now let us describe stress relaxation behaviour. Consider the applied strain to be instantaneous and constant:

$$\varepsilon(t) = \varepsilon_o e_o(t) \tag{2.14}$$

Hence, the the time-dependent stress from Hooke's law gives:

$$\sigma(t) = M(t)\varepsilon_o \tag{2.15}$$

For a simple visco-elastic system with a single relaxation time, the modulus for the stress relaxation is described as follows:

$$M(t) = M_o\delta(t) + M_\infty + \sum_k \Delta M_k(e^{-\frac{t}{\tau_{\varepsilon k}}}) \tag{2.16}$$

The generalised continuous relaxation time spectrum is thus:

$$M(t) = M_\infty + \int_{-\infty}^{\infty} H(ln\ \tau)\, e^{\frac{-t}{\tau}}\, \mathrm{d}\, ln\tau \tag{2.17}$$

By assuming that the pure viscous flow processes are negligable, the system experience only the elastic and relaxation component. Thus, when $t \to \infty$, the fundamental equation for a simple relaxing body can be obtained:

$$\frac{\sigma_\infty}{\varepsilon_\infty} = M_\infty \tag{2.18}$$

$$\dot{\varepsilon} = \frac{1}{\tau_\varepsilon}(\varepsilon_\infty - \varepsilon) \tag{2.19}$$

$$\dot{\sigma} = \frac{1}{\tau_\sigma}(\sigma_\infty - \sigma) \tag{2.20}$$

$$\sigma + \tau_\sigma \dot{\sigma} = M_\infty(\varepsilon + \tau_\varepsilon \dot{\varepsilon}) \tag{2.21}$$

2.4.2 Dynamic deformation
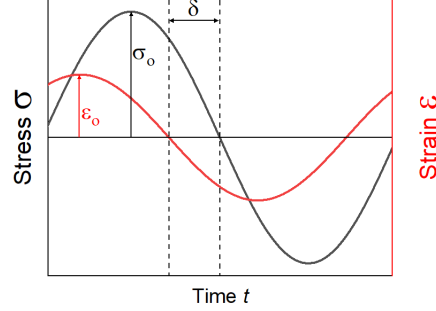
FIGURE 2.7: Periodic sinusoidal deformation with the corresponding strain response.

The working principle of a typical dynamic deformation experiment is shown in figure 2.7. For a visco-elastic system, there is an inherent phase lag δ between the applied stress and the strain response. For a period system of frequency ω, the stress and strain can be defined as follows:

$$\sigma(t) = \sigma_o e^{i\omega t} \tag{2.22}$$

$$\varepsilon(t) = \varepsilon_o e^{i\omega t - \delta} \tag{2.23}$$

Substituting the periodic stress and strain definition in equation 2.22 and 2.23 respectively into the equation of a simple relaxation body of equation 2.21, the following relation is obtained:

$$\sigma(1 + i\omega t_\sigma) = M_o \varepsilon(1 + i\omega \tau_\varepsilon) \tag{2.24}$$

Assuming that the system goes into an equilibrium state at $t \to \infty$, the modulus at infinity M_∞ is given as:

$$M_\infty = \frac{\sigma(\omega \to \infty)}{\varepsilon(\omega \to \infty)} = M_o \frac{\tau_\varepsilon}{\tau_\sigma} \tag{2.25}$$

Note that $M_\infty > M_o$, hence τ_ε is always larger than τ_σ. Resolving equation 2.24, the complex expression of the modulus is obtained:

$$M^*(\omega) = \frac{\sigma(\omega)}{\varepsilon(\omega)} = M'(\omega) + iM''(\omega) \tag{2.26}$$

TABLE 2.2: Dimension comparison between RLC circuit and mechanical oscillator[33].

RLC circuit	Mechanical oscillator
Charge, q	Amplitude, x
Current, I	Velocity, v
Inductance, L	Mass, m
Resistance, R	Damping constant, γ
Capacitance, C	Inverse spring constant, k^{-1}
EMF, ε	Driving force, F(t)

$$M'(\omega) = M_o + \Delta M \frac{\omega^2 \tau^2}{1 + \omega^2 \tau^2} \tag{2.27}$$

$$M"(\omega) = \Delta M \frac{\omega \tau}{1 + \omega^2 \tau^2} \tag{2.28}$$

2.5   Harmonic Oscillator

A body is said to exhibit simple harmonic motion when the force acting on it is directly proportional to the displacement from the mean position and is always directed to the mean position [32]. In nature, the magnitude of the restoring force continuously decays as the body loses energy to the environment. Hence, in classical mechanics terms, the harmonic oscillation of system can be represented by a spring and dash-pot system. The former is representative of the restoring force and the latter as a means to introduce a damping behaviour.

This is a universal concept and is also found in electrical systems such as an RLC circuit, the simplest form of electrical harmonic oscillator. The capacitor, C, and inductor, L, serves as the restoring force, transforming from an electric to a magnetic field. The resistor, R provides a damping characteristic, similar to the dash-pot of the aforementioned mechanical system. A summary of the physical units are shown in table 2.2.
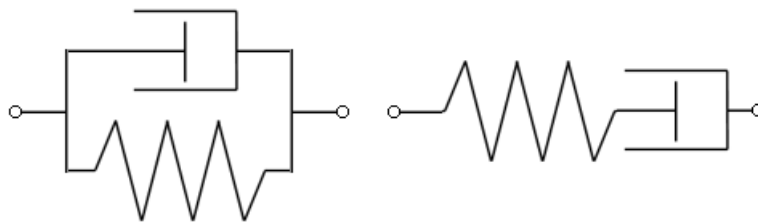
FIGURE 2.8: The Kevin-Voigt model (left) and Maxwell model (right).

For a visco-elastic material like rubber, there are two fundamental visco-elastic model used: the Maxwell model and the Kevin-Voigt model. The setup of these models are shown in figure 2.8. The Maxwell model is able to exhibit the stress relaxation due to the force being constant across the two visco-elastic component, and the strain deformation is distributed. This equal strain distribution

however leads to a strain or extension of the system to be intrinsically linear which does not occur in reality. The Kevin-Voigt model resolves this by having the applied strain as invariable and henceforth the stress distributed. This allows the observation of the creep behaviour, but at the cost of exhibiting an instantaneous stress response.The two subsequent sub-chapters are dedicated to further elaborate model description.

2.5.1 Maxwell Model

$$\sigma = \sigma_{spring} = \sigma_{dashpot} \tag{2.29}$$

$$\varepsilon = \varepsilon_{spring} + \varepsilon_{dashpot} \tag{2.30}$$

Combining the first order time derivative of equation 2.30, $\sigma = E\epsilon$ and $\tau = \eta\dot{\gamma}$, the following equation is obtained:

$$\dot{\varepsilon} = \frac{\dot{\sigma}}{G} + \frac{\sigma}{\eta_{dashpot}} \tag{2.31}$$

Note that the modulus G replaces the modulus E as dynamic experiments are often performed in shear deformation mode. Defining the stress and strain periodically as in equation 2.22 and 2.23, equation 2.31 then becomes:

$$i\omega\varepsilon = \sigma\left(\frac{i\omega}{G} + \frac{1}{\eta}\right) \tag{2.32}$$

Finally, using the complex modulus definition in equation 2.26, the real, imaginary and loss tangent is given as:

$$G^*(\omega) = \frac{i\omega\eta}{1 + i\omega\tau} \ with \ \tau = \frac{\eta}{G} \tag{2.33}$$

$$G'(\omega) = G\frac{\omega^2\tau^2}{1 + \omega^2\tau^2} \tag{2.34}$$

$$G"(\omega) = G\frac{\omega\tau}{1 + \omega^2\tau^2} \tag{2.35}$$

$$tan \ \delta = \frac{1}{\omega\tau} \tag{2.36}$$

As previously stated, this model is unable to account for the time-dependent creep behaviour.

2.5.2 Kevin-Voigt Model

$$\varepsilon = \varepsilon_{spring} = \varepsilon_{dashpot} \tag{2.37}$$

$$\sigma = \sigma_{spring} + \sigma_{dashpot} = \eta\dot{\varepsilon} + G\varepsilon \tag{2.38}$$

As was the case for the Maxwell model, defining the stress and strain periodically as in equation 2.22 and 2.23, the equation then becomes:

$$\sigma = (i\omega\eta + G)\varepsilon \tag{2.39}$$

Hence, the real, imaginary and lost tangent equation can be easily extracted in combination with the definition of modulus in equation 2.26:

$$G'(\omega) = G \tag{2.40}$$

$$G"(\omega) = \omega\eta \tag{2.41}$$

$$tan\,\delta = \omega\tau \tag{2.42}$$

Since the complex compliance J is the reciprocal of the complex modulus, $J^* = \frac{1}{G^*}$, the real and imaginary part of the compliance is as follows:

$$J' = \frac{J}{1 + \omega^2\tau^2} \tag{2.43}$$

$$J" = J\left(\frac{\omega\tau}{1 + \omega^2\tau^2}\right) \tag{2.44}$$

As previously stated, this model is unable to account for the stress relaxation.

2.6 Transmissibility ratio

The transmissibility of a given system can be defined as the ratio of the output and input signal [34]. Let the equation of motion for the Zener model (a combination of Kevin-Voigt and Maxwell model) as shown in figure 2.9 be defined as follows:
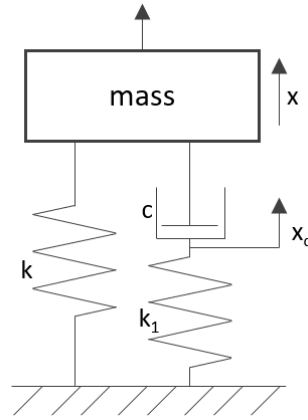
FIGURE 2.9: The Zener model

$$\frac{d^2x}{d\tau^2} + x + 2\xi\left(\frac{dx}{d\tau} - \frac{dx_d}{d\tau}\right) = \frac{F(\Omega)}{k}$$
$$2\xi\left(\frac{dx}{d\tau} - \frac{dx_d}{d\tau}\right) = \gamma x_d$$

(2.45)

where $\tau = \omega_n t$, $\gamma = k_1/k$, $\Omega = \omega/\omega_n$, ω is the excitation frequency and $\frac{F(\Omega)}{k}$ is a type of forcing (only Kevin-Voigt is shown):

a) Mass Excitation:
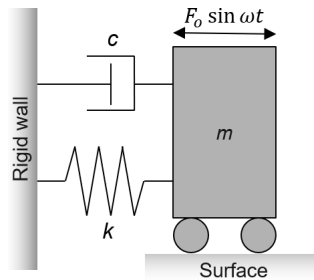
FIGURE 2.10: Single degree-of-freedom system for mass excitation

$$\frac{F(\Omega)}{k} = g_1(\Omega)e^{i\Omega\tau} \;\; where \; g_1(\Omega) = \frac{F_o}{k}$$

(2.46)

b) Base Excitation:

$$\frac{F(\Omega)}{k} = y_o(1 + i2\xi\Omega)e^{i\Omega\tau} = g_2(\Omega)e^{i\Omega\tau}$$
$$where \; g_2(\Omega) = y_o\sqrt{1 + (2\xi\Omega)^2}e^{i\phi_b} \;\; , \;\; \phi_b = tan^{-1}(2\xi\Omega)$$

(2.47)

c) Rotating Unbalanced Mass:
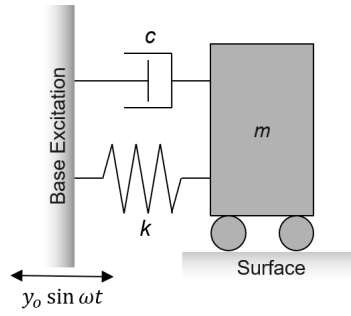
FIGURE 2.11: Single degree-of-freedom system for base excitation
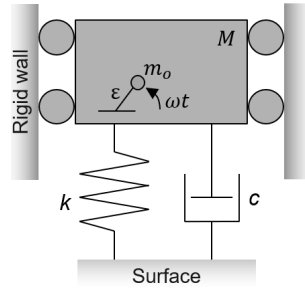
FIGURE 2.12: Single degree-of-freedom system for rotating unbalance mass

$$\frac{F(\Omega)}{k} = g_3(\Omega)e^{i\Omega\tau}$$

$$where\ g_3(\Omega) = \frac{m_o\epsilon}{M + m_o}\Omega^2 \ , \ \omega_n = \sqrt{\frac{k}{M + m_o}} \tag{2.48}$$

Assume that the solution of the differential equation for equation 2.45:

$$x(\tau) = X_p(\Omega)e^{i\Omega\tau}$$

$$x_d(\tau) = X_{p,d}(\Omega)e^{i\Omega\tau} \ p = 1, 2, 3 \tag{2.49}$$

Substituting equation 2.49 into equation 2.45 (subscript p represents the excitation mode described above) and solving X_p and $X_{p,d}$:

$$X_p(\Omega) = \frac{\gamma + i2\xi\Omega}{a_o + ib_o}g_p(\Omega)$$

$$X_{p,d}(\Omega) = \frac{i2\xi\Omega}{a_o + ib_o}g_p(\Omega) \ p = 1, 2, 3$$

$$where \ a_o = \gamma(1 - \Omega^2)$$

$$b_o = 2\xi\Omega(1 + \gamma - \Omega^2) \tag{2.50}$$

Expressing the above formula in exponential form:

$$X_p(\Omega) = H_M(\Omega)g_p(\Omega)e^{i\theta_M(\Omega)}$$

$$X_{p,d}(\Omega) = H_{dM}(\Omega)g_p(\Omega)e^{i\theta_{dM}(\Omega)} \ p = 1, 2, 3 \tag{2.51}$$

Where

$$H_M(\Omega) = \sqrt{\frac{\gamma^2 + (2\xi\Omega)^2}{a_o^2 + b_o^2}} = \sqrt{\frac{\gamma^2 + (2\xi\Omega)^2}{\gamma^2(1-\Omega^2)^2 + (2\xi\Omega)^2(1+\gamma-\Omega^2)^2}}$$

$$H_{dM}(\Omega) = \frac{2\xi\Omega}{\sqrt{a_o^2 + b_o^2}} = \frac{2\xi\Omega}{\sqrt{\gamma^2(1-\Omega^2)^2 + (2\xi\Omega)^2(1+\gamma-\Omega^2)^2}}$$

$$\theta_M(\Omega) = tan^{-1}\left(\frac{2\xi\Omega a_o - \gamma b_o}{\gamma a_o + 2\xi\Omega b_o}\right) = tan^{-1}\left(\frac{-2\xi\Omega\gamma^2}{\gamma^2(1-\Omega^2)^2 + (2\xi\Omega)^2(1+\gamma-\Omega^2)^2}\right)$$

$$\theta_{dM}(\Omega) = tan^{-1}\left(\frac{a_o}{b_o}\right) = tan^{-1}\left(\frac{-\gamma(1-\Omega^2)}{2\xi\Omega(1+\gamma-\Omega^2)}\right)$$

(2.52)

As $\gamma \to \infty$ (whereby k_1 is considered rigid), the Maxwell model is thus reduced to the Kelvin-Voigt model:

$$\lim_{x\to\infty} H_M(\Omega) \to \frac{1}{\sqrt{(1-\Omega^2)^2 + (2\xi\Omega)^2}}$$

$$\lim_{x\to\infty} H_{dM}(\Omega) \to 0$$

(2.53)

Therefore based on the method of excitation, a specific amplitude and phase response can be obtained:

a) Mass excitation

$$\frac{d^2x}{dt^2} + \omega_n^2 x + 2\xi\omega_n\left(\frac{dx}{dt} + \frac{dx_d}{dt}\right) = \frac{F_o}{m} sin\,\omega t$$

$$2\xi\left(\frac{dx}{dt} - \frac{dx_d}{dt}\right) = \gamma\omega_n x_d, \quad where \quad \omega_n = \sqrt{\frac{k}{m}}$$

(2.54)

$$\therefore x(t) = \frac{F_o}{k} H_M\,sin\,(\omega t - \theta_M)$$

(2.55)

b) Base excitation

$$\frac{d^2x}{dt^2} + \omega_n^2 x + 2\xi\omega_n\left(\frac{dx}{dt} + \frac{dx_d}{dt}\right) = 2\xi y_o \omega \omega_n\,cos\omega t + y_o \omega_n^2\,sin\,\omega t$$

$$2\xi\left(\frac{dx}{dt} - \frac{dx_d}{dt}\right) = \gamma\omega_n x_d, \quad where \quad \omega_n = \sqrt{\frac{k}{m}}$$

(2.56)

$$\therefore x(t) = y_o\sqrt{1 + (2\xi\omega/\omega_n)^2} H_M\,sin\,(\omega t - \theta_M + tan^{-1}\,2\xi\omega/\omega_n)$$

(2.57)

c) Rotating unbalance mass

$$\frac{d^2x}{dt^2} + \omega_n^2 x + 2\xi\omega_n\left(\frac{dx}{dt} + \frac{dx_d}{dt}\right) = \frac{m_o\epsilon}{M + m_o}\omega^2\,sin\,\omega t$$

$$2\xi\left(\frac{dx}{dt} - \frac{dx_d}{dt}\right) = \gamma\omega_n x_d, \quad where \quad \omega_n = \sqrt{\frac{k}{M + m_o}}$$

(2.58)

$$\therefore x(t) = \frac{m_o \epsilon}{M + m_o} \frac{\omega^2}{\omega_n^2} H_M \, sin \, (\omega t - \theta_M) \tag{2.59}$$

In the current experimental setup, the base excitation mode (2.57) was utilised.

2.7 Nonlinearity in rubber compounds

As shown in the typical Payne curve (log G' vs log ω), the are two distinct region of material response with respect to strain, the linear viscoelastic (LVE) region, where the modulus is invariant to the applied strain, and the nonlinear viscoelastic (NVE) region. Experimentally, the latter is due to the appearance of higher harmonics embedded in the material response to deformation. It could be approximated by Taylor series expansion:

$$G^* = a_0 + a_1 \gamma + a_2 \gamma^2 + a_3 \gamma^3 + a_4 \gamma^4 + ...$$

$$where \; a_i \; are \; complex \; numbers \tag{2.60}$$

As a general case, the stress measurement with respect to the shear amplitude can be described as follows:

$$\begin{aligned} \sigma &= G^* \gamma_0 e^{i(\omega t)} \;\; with \;\; \gamma = \gamma_0 e^{i(\omega t)} \\ &= [a_0 + a_1 \gamma + a_2 \gamma^2 + a_3 \gamma^3 + a_4 \gamma^4 + ...] \gamma_0 e^{i(\omega t)} \\ &= a_0 \gamma_0 e^{i(\omega t)} + a_1 \gamma_0^2 e^{i(\omega t)} + a_2 \gamma_0^3 e^{i(\omega t)} + a_3 \gamma_0^4 e^{i(\omega t)} + ... \end{aligned} \tag{2.61}$$

Large amplitude oscillatory shear (LAOS) technique was designed to characterise the degree of nonlinearity while obtaining physically meaningful interpretation. There are several analytical approaches such as: the moduli as a function of strain amplitude, the stress shape (e.g. Lissajous-Bowditch curve) and via Fourier analysis [7]. The latter is known as FT-Rheology and was developed by Wilhelm et al.

In FT-Rheology, only odd higher-order terms are theoretically obtainable from equation 2.61. This is due to the nature of shearing deformation and therefore the symmetry criteria for LAOS is given in equation 2.62. The even higher-order terms could still arise from the experimental setup such as inhomogeneous material flow in the measuring cavities (wall-slip) and the imperfections of the mechanical excitation.

$$\sigma[-\gamma(t), -\dot{\gamma}(t)] = -\sigma[\gamma(t), \dot{\gamma}(t)] \tag{2.62}$$

Wilhelm et al. had used the relative intensity of the third harmonic $I_{3/1}$ to characterise the material nonlinearity that could arise from the degree of branching for polymer chains, dispersion of colloid system to name a few [7].

$$I_{3/1} = \frac{I_3}{I_1} \tag{2.63}$$

The influence of carbon black in rubber compounds has been investigated by Schwab and Wilhelm via LAOS method [35]. Three different carbon black grades with various specific surface area were investigated as a function of concentration in an unvulcanised SBR. When normalising the carbon black with its corresponding oil adsorption number, the three $I_{3/1}$ curves could be normalised into a single filler-induced curve. This suggests the direct influence of filler aggregate properties in the compound's nonlinear response.

All the description above pertains to samples under high deformation and low frequency as this gives the best experimental resolution. In the current investigation, the nonlinearity effects under relatively high frequency and low deformation is explored since it is known from rubber science that its property is a function of strain, deformation mode and frequency/temperature. This is performed with the aid of a resonance-based measurement technique, which would give the best signal to noise ratio when compared to a conventional dynamic mechanical analysis (DMA).

Chapter 3

Methodology

3.1 TSSR
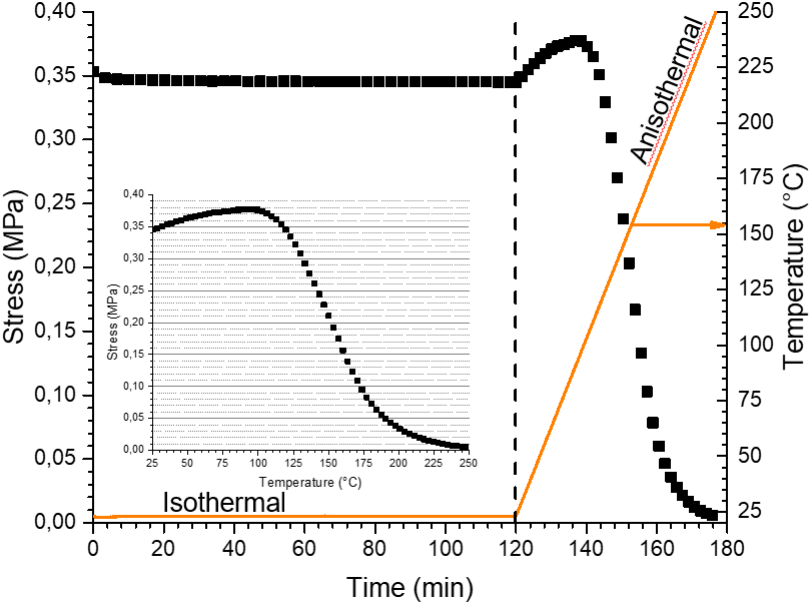
FIGURE 3.1: An example of experimental unfilled NR results obtained from TSSR. The inset is the isothermal result with the abcissa as temperature.

The temperature scanning stress relaxation (TSSR) is essentially a temperature-dependent mechanical creep experiment. Developed by Brabender, Duisburg, Germany, the device is able to apply strain levels up to 100% while the temperature ramp has a maximum heating rate of 4K/min. The sample type is based on the standard S2 specimen as specified by DIN53504. As shown in figure 3.1, the experiment is separated into two stages, the isothermal and anisothermal step. The first step is essentially performed to allow the system to relax with the user-defined strain conditions at isothermal conditions, in order to have the same baseline values when compared to other systems. Once a baseline value is obtained, a temperature ramp is applied and the stress relaxation is recorded. These stress relaxations could be distinguished between the polymer-filler and the polymer network interactions which contributes to the stress response of the rubber sample.

Based on the relaxation spectrum of a quasi-static experiment (see chapter 2.4.1), the time dependent modulus can be written as follows:

$$E_{iso}(t) = E_{\infty} + \int_{-\infty}^{\infty} H(\tau)\, e^{\frac{-t}{\tau}} \, \mathrm{d}\, ln\tau \tag{3.1}$$

Where $E_{iso}(t)$ is the isothermal Young's modulus at time t, H is the relaxation spectrum and τ is the relaxation time constant.

According to Alfrey's law [36], differentiating $E_{iso}(t)$ with respect to $ln\,\tau$, the relaxation spectrum time constant is equivalent to the time decay, $H(\tau)$ at $\tau = t$:

$$H(\tau) = -\left(\frac{dE_{iso}}{d\,lnt}\right)_{t=\tau} = -t\left(\frac{dE_{iso}}{dt}\right)_{t=\tau} \tag{3.2}$$

In the experimental setup, a heating rate β is applied and the final relaxation spectrum description is as follows:

$$H(T) = -\Delta T \left(\frac{dE_{non-iso}}{dT}\right)_{\beta=\frac{\Delta T}{t}=constant} \tag{3.3}$$

When plotting the relaxation spectrum against temperature, material response from different components can be observed such as polymer network and filler network [37–40].

3.2 Conventional DMA

First proposed by Poynting in 1909 [18, 41], the dynamic mechanical analysis DMA is a technique that measures the viscoelastic behaviour of a material. In the simplest experimental setup, a disc-shaped sample is placed in between an actuator and a force sensor. The actuator then perturbates the sample sinusoidally either in terms of a force or strain constant. The mechanical signal that passes through the material is received at the sensor and is then compared to the original signal that was induced by the actuator. The comparison between the input and the corresponding output signals is the basis of the material characterization (see chapter 2.4.2). In the present work, DMA-Eplexor 2000N by Netzsch Gabo Instruments, Ahlden, Germany were used.

3.3 High Frequency DMA

The high frequency DMA measurements were performed on the VHF104 device (Metravib, Lyon, France). The measurable frequency window is between 100 Hz to 10 kHZ, with the maximum acceleration of 200 m/s^2. Since it is a resonant vibration approach, the resonance of the sample

(disc-shaped) must be tuned in order to fully realise the wide frequency window. The resonance frequency f_o can be determined with following equation:

$$f_o = \frac{1}{2\pi}\sqrt{\frac{E \cdot S}{l \cdot M}} \tag{3.4}$$

Where E is the Young's modulus in N/m^2, S the cross-sectional contact area in m^2, l the height of the sample in m and M is the added top mass in kg.

As previously mentioned, the forced resonant vibration approach is based analysing the resonance peak from the transmissibility curve. The experimental setup is based on the base excitation of the system (see chapter 2.6). Therefore from equation 2.57, the transmissibility ratio from the VHF machine is given as equation 3.5:

$$Transmissibility = \frac{F_{transmitted}}{F_{excited}} = \sqrt{\frac{1 + \left(2 \cdot \xi \cdot \Omega\right)^2}{\left(1 - \Omega^2\right)^2 + \left(2 \cdot \xi \cdot \Omega^2\right)^2}} \tag{3.5}$$

Where $F_{transmitted}$ and $F_{excited}$ are transmitted and excited force respectively, ξ is the damping coefficient and Ω is the resonance-normalised frequency.

3.4 Microscopy

In the present work, two types of microscopy techniques were used to characterise the filler network. The following subsections are dedicated to the Transmission Electron Microscope (TEM) and Atomic Force Microscope (AFM).

3.4.1 Transmission Electron Microscope

TEM operates with the same principle as a light microscope but instead utilises an electron beam as oppose to a visible light beam. Based on the wave-particle dualism, an electron particle can be described with the de Broglie wavelength $\lambda_{deBroglie}$:

$$\lambda_{de\ Broglie} = \frac{h}{m_e \nu_e} \tag{3.6}$$

This infers that the velocity of the electron ν_e has a direct influence on $\lambda_{deBroglie}$ since the mass of the electron m_e and Planck constant h are invariants. Hence increasing the voltage of the electron emission, different wavelengths are generated. These wavelengths dictates the smallest distance d_d (theoretical resolution) that can be resolved is described by the Rayleigh criterion:

$$d_d = 1.22\frac{\lambda}{\alpha} \tag{3.7}$$

where α is the convergence beam and λ is the wave length.

In TEM, there are two fundamental approaches in creating an image contrast: amplitude and phase contrast. As the name implies, the amplitude contrast deals with the number of scattered electron, while the phase contrast is a measurement of the phase shift due to the difference in wave path length. Within amplitude contrast, there are two principle types: mass-thickness contrast and diffraction contrast [42–44]. The latter uses scattering designated at special Bragg angles, whereby the incident electron beam experiences constructive interference. In the current investigation, mass-thickness contrast was utilised.

The basis of the mass-thickness contrast is the incoherent elastic scattering of electrons. This mode is often used in amorphous samples as there are no diffraction contrast that could arise due to lack periodicity/crystallinity. Rutherford scattering function is given as follows:

$$f(\theta) = \frac{(1 + \frac{E_o}{m_o c^2})}{8\pi^2 a_o}(\frac{\lambda}{sin\frac{\theta}{2}})^2(Z - f_x) \tag{3.8}$$

where Z is the atomic number of the sample, excitation energy E_o and de Broglie's wavelength λ is a function of voltage, and f_x is the scattering factor of X-rays.

The image contrast C, which is the ratio of the changes of intensity ΔI with respect to beam source intensity I, is given as:

$$C = \frac{\Delta I}{I_{input}} = 1 - exp^{-\sigma\rho t} \tag{3.9}$$

Here, ρ is defined as the material density, t is the sample thickness and σ is the scattering cross section, which is a function of atomic number Z and acceleration voltage.

The TEM analysis was performed on a JEM1400 instrument (Jeol, Tokyo, Japan) using a voltage of 100 kV. The CB network structures were investigated by measuring the sample in both swollen as well as the bulk state. For the swollen state, the sample is first extracted with acetone in order to remove any unbound additives via soxhlet extraction. After drying at 70°C for two hours, the extracted sample is then swollen to equilibrium in a styrene/benzoyl peroxide solution being polymerised at 70°C [45]. Finally, ultramicrotomic slices of approximately 60 nm are prepared from both the swollen and bulk state by using a cryo-ultramicrotome (Leica EM UC6/EM FC6) equipped with a diamond knife.

3.4.2 Atomic Force Microscope

An AFM is a mechanical imaging instrument that measures the three dimensional topography as well as physical properties of a surface with a sharpened probe at the end of a flexible cantilever.

The radius of the cantilever probe is in the range nanometer, and is guided along a defined grid (raster-like) over the surface of the sample. When the probe head is positioned closed enough to the sample surface, it is able to interact with the force fields associated with surface. These interactions would then deflect the cantilever with respect to the forces it experiences. With the aid of a laser system that is positioned independently to the cantilever, the position of the cantilever can be acquired with the reflected laser beam onto photo-sensitive diodes.

In terms of precision, the AFM is able to detect the force interactions in the order of 10^{-6} and 10^{-11} N [46]. The cantilever probe is able to experience either attractive interactions (Van der Waals, dipole dipole or electrostatic interactions) or a repulsive forces (Coulomb interactions) [47] based on the distance with the sample surface. This phenomena is explained using the Lennard-Jones potential as shown in figure 3.2. Therefore based on the area of interest, three standard operating can be used to characterise the surface interactions: Contact mode, Non-contact mode and Intermittent contact mode.
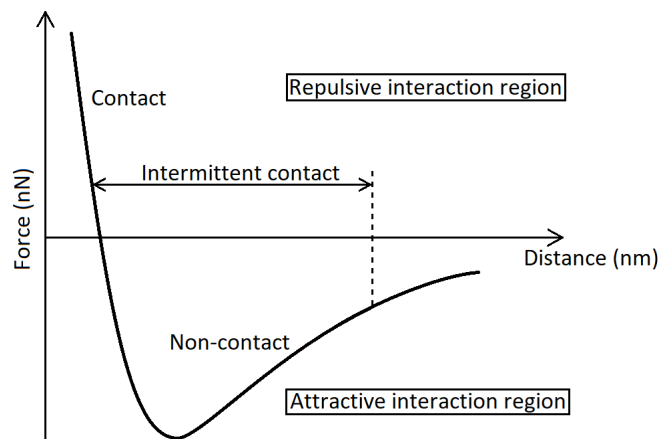
FIGURE 3.2: The schematic of the Lennard-Jones potential with the corresponding regions of AFM modes.

In the AFM Contact mode, the probe is in constant contact with the surface and is essentially dragged over the surface of the sample with a fixed deflection. The height of the probe is adjusted through a force feedback system which enables a topography imaging. Due to the nature of this mode, the probe tip deteriorates relatively quick and henceforth a degradation of the image resolution after prolong usage [48].

In the AFM Non-contact mode, the probe oscillates with a small amplitude near the sample surface, without coming into contact with it. The change in amplitude is compensated by the measuring device and is used to construct the topography. This enables a higher image resolution without destroying the tip, under high vacuum. If performed in ambient conditions, the probe tends to crash into the sample surface due to capillary force and could potentially damage both the probe head and sample surface.

In an Intermittent contact mode, the cantilever oscillates at a larger amplitude, with the aim of experiencing both attractive and repulsive forces. When compared to the contact mode, the probe

is in contact with the surface for a significantly shorter time and thus experiences lower lateral shear forces. This enables a higher image resolution[48]. The drawback of this mode is that the force between the probe and the sample surface cannot be controlled directly.

In the present work, a special Intermittent contact mode called "Peak Force Quantitative Nanomechanical Mapping" (PF-QNM) was used. In this mode, the cantilever oscillates with a maximum amplitude at a defined frequency between 1 to 10 kHz. As the cantilever approaches and retracts from the sample surface, a force-displacement curve is generated as shown schematically in figure 3.3. From this plot, various material properties such as modulus, adhesion and dissipation can be extracted.
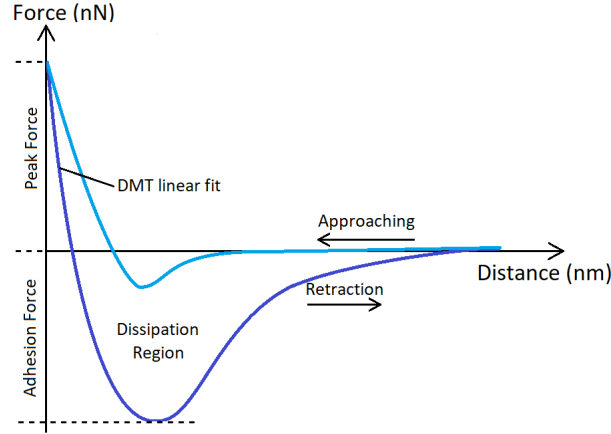
FIGURE 3.3: A schematic of the force-displacement curve acquired by PF-QNM mode.

The modulus is determined by fitting the linear portion of the retraction curve and utilising the Derjaguin-Muller-Toporov (DMT) model [49]:

$$F = \frac{4}{3} E^* \sqrt{R \delta^3} + F_{Adh} \tag{3.10}$$

The DMT model is an extension to the Hertzian model, with addition the adhesion force, F_{Adh}. Taking into consideration the radius of the probe tip, R and the indentation depth of the sample δ, the reduced modulus E* can be obtained. E* can be then transformed into the sample modulus E_s utilising the following equation:

$$E_s = \frac{3(F - F_{Adh})(1 - \nu_s^2)}{4\sqrt{R \delta^3}} \tag{3.11}$$

Note that the Poisson's ratio of the sample ν_s is often taken as 0.5 for incompressible material such as rubber.

In the present work, the AFM measurements were performed on a Dimension Icon AFM instrument provided with a NanoScopeV controller from Bruker (Santa Barbara,California, USA). Similar to the sample preparation for TEM, the samples were extracted beforehand to avoid blooming effects on the sample surface and sample slices were made with the cryo-ultramicrotome.A constant

oscillating frequency were used under ambient conditions using a cantilever (RTESPA-150) probe with a nominal spring constant of 6 N/m and a tip radius of 8 nm. Finally, A scanning area of 5×5 μm^2 was used for an overview of the sample properties, and an area of 2×2 μm^2 was chosen for a detailed view. In both cases, the image resolution was set to 256×256 pixels.

Chapter 4

Results and Discussion

This section is separated into three parts based on the peer-reviewed publications; characterization of the reinforcing resin mechanism, the Fourier analysis of the vibrational resonance and the material nonlinearity of filled systems.

4.1 Characterizing the influence of reinforcing resin on the structure and the mechanical response of filled isoprene rubber

The article [50] was published with the focus of utilizing various experimental approaches to develop a deeper insight in the reinforcing resin mechanism in rubber compounds. Resorcinol was used as a model ingredient since it is widely used in the tire industry.

The main outcome from this investigation is that the reinforcing resin reacts with the interface of the carbon black, hence making the filler network more compact. This is reflected in the lowering of the filler percolation threshold and the enhancement of the Payne effect, whereby the breakdown of the filler network due to strain is significantly reduced. Images obtained from the AFM and TEM were utilised to reaffirm the main statement of the investigation.

Due to copyright, the article can be accessed at https://doi.org/10.1080/1539445X.2018.1509872

4.2 Nonlinearity in the Mechanical Response of Rubber as Investigated by High-Frequency DMA

The second paper [51] introduces a novel method of characterising the nonlinearity of a rubber compound. It is the first instance of the superharmonic resonance phenomenon reported in the Fourier space of the transmissibility curve of rubber.

In the first section, the data processing step is reported with the emphasis of extracting relevant Fourier data points. The subsequent section elaborates the appearance of the superharmonic resonances within the experimental data after the data processing step is performed. Two distinct nonlinearities in terms of filler dependencies were observed, polymer induced nonlinearity below the filler percolation threshold, and filler induced nonlinearity above the percolation threshold. Finally, the appearance of the foldover effect was noted and modelled with cubic nonlinear system derived from the Kelvin-Voigt model. The α-parameter extracted from the aformentioned model, was then used to compare with the nonlinearity observed from the superharmonic resonances. Both approaches had shown similar results, though the latter is deemed to be more sensitive due to the quantification of the polymer induced nonlinearities.

MDPI

Nonlinearity in the Mechanical Response of Rubber as Investigated by High-Frequency DMA

Imran Hussain Syed [1,*] , Pascal Vouagner [2], Frank Fleck [1] and Jorge Lacayo-Pineda [1]

[1] Continental Reifen Deutschland GmbH, Jaedekamp 30, 30419 Hannover, Germany;
Frank.fleck@conti.de (F.F.); jorge.lacayo-pineda@conti.de (J.L.-P.)

[2] Metravib, 200 Chemin des Ormeaux, F-69578 Limonest, France; pascal.vouagner@acoemgroup.com

* Correspondence: imran.syed@conti.de

check for updates

Abstract: Nonlinear material response is analysed with the Fourier transform (FT) of the raw signal measured by a high-frequency dynamic mechanical analyzer (HF DMA). It is known from rheological behaviour of elastomers that reinforcing fillers additionally induce nonlinearity in an already inherently nonlinear system. This behaviour is often described in terms of a mechanical response of strain sweeps, essentially the transition from the linear viscoelastic (LVE) to the nonlinear viscoelastic (NVE) region. In the current investigation, the NVE region could be observed with respect to frequency under low-amplitude deformation. A foldover effect was observed, whereby the material exhibited a nonlinear dependency in relation to the increment of the filler amount above the percolation threshold. In addition, an apparent superharmonic resonance was observed within higher orders of vibrational modes which is further indication of nonlinearity. In this paper, the analytical approach is presented as a novel method to characterise the behaviour of the polymer–filler interaction by HF DMA.

Keywords: nonlinearity; superharmonic resonance; foldover effect; HF DMA

1. Introduction

Rubber is one of the most prevalent among the materials in our daily life that exhibit mechanical nonlinearity. Even with this familiarity, deep understanding of this material remains a substantial challenge to this very day. A common way to characterise rubber is with the dynamic mechanical analyzer (DMA). The basic principle behind this technique is the measurement of the difference between the excitation signal and the material's response as a function of both deformation and time. A material is defined as more viscous (or rubbery) when the difference between these parameters is large [1].

All elastomers have a region whereby the modulus of the system is independent of the strain applied. However, after a certain strain threshold the modulus drops significantly with respect to the applied amplitude. This is mainly due to the rearrangement of the polymer chains with respect to the external applied force, and is also reflected in the stress–strain curve, where the mechanical response portrays a non-Hookean behaviour [2]. The introduction of fillers lowers the critical strain threshold and is caused by a combination of the hydrodynamic reinforcement of the filler particles and the formation of a filler network [3]. The breakdown of this filler network is described as the so-called "Payne effect" [4].

In a routine DMA measurement, a simple linear viscoelastic material is assumed, whereby only the absolute amplitude and phase shift of the signals are taken into consideration. In reality, however, these signals are rarely ideally sinusoidal and are a convolution of both the imperfection derived from the oscillator as well as the nonlinearity of the material. Assuming that the imperfection of the

oscillator is minimal, these signal distortions can be used to describe the material in greater detail. This method is known as Fourier transform (FT) rheology and has been developed by various research groups [5–7].

Recently, systematic investigations of the influence of fillers in rubber have been performed by Wilhelm et al. whereby the experimental raw signals from amplitude variation up to very large deformations were converted into Fourier space, hence decomposing the distortion into quantifiable signals. These decomposed signals show a strong dependency on the amount and types of reinforcing fillers present in the material [8,9]. The main parameter used to distinguish the filler-induced nonlinearities is the intensity ratio of the third to the first harmonic response in Fourier space, $I_{3/1}$ [10].

In analogy, instead of amplitude variation, the raw data obtained by frequency variation was analysed in Fourier space under low-amplitude deformation. While the strain dependency of nonlinearity has been extensively investigated, the frequency behaviour at low strain amplitude is often assumed to be completely linear, and some clarification is therefore needed. In addition, the current method based on strain sweeps requires uncured rubber, while cured rubber is utilised in the present investigation, as it is the state linked to the final application of rubber products. Henceforth, this paper can be categorised into three sections: the data treatment, where all the analytical steps are shown; the vibrational superharmonics; and the foldover effect. These effects are the consequence of the nonlinearity effects of the material [11].

2. Materials and Methods

A VHF104 high-frequency DMA (Metravib, Lyon, France), as shown in Figure 1, was used in the current investigation. The sample was glued between two metal cylinders, one acting as a base and the other to deliver a preload force onto the sample. The main advantage of this device is the ability to measure frequencies up to 10 kHz, which is not possible with a traditional DMA device (typically up to 100 Hz). This DMA is a type of forced vibration resonant system, according to ASTM D5992 [12], essentially using the resonance principle to evaluate the mechanical response of the material. The data are presented in a transmissibility plot as shown in Figure 2. The figure was generated by using the transmissibility formula in Equation (1), where ξ is the damping ratio of the system and Ω is the resonance-normalised frequency of the system:

$$Transmissibility = \frac{F_{transmitted}}{F_{excited}} = \sqrt{\frac{1 + \left(2 \cdot \xi \cdot \Omega\right)^2}{\left(1 - \Omega\right)^2 + \left(2 \cdot \xi \cdot \Omega\right)^2}} . \tag{1}$$
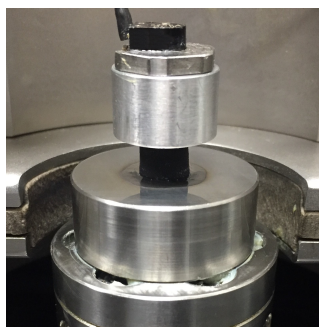
Figure 1. The experimental setup for the VHF104 dynamic mechanical analyzer.

The experimental setup was essentially comprised of two components: the base excitation input and the top transmission output, as illustrated in Figure 3. The viscoelastic properties of a material can be approximated in terms of a spring (elastic component) and a dashpot (viscous component) [13]. The base excitation generates a defined, constant excitation that passes through the sample, and the transmitted signal is received on the accelerometer located at the head of the top mass.

Figure 2. An example of the transmissibility curve generated from Equation (1), with various damping factors.

Figure 3. Basic schematic for the current experimental setup.

Resonance occurs when a perturbation frequency matches a system with its natural frequency. Under resonance, the system is able to exhibit dynamics with a larger amplitude than the initial perturbation state. The transmissibility curve, which is a measure of the maximum amplitude response normalised to the maximum amplitude of the input, is one of many ways to repres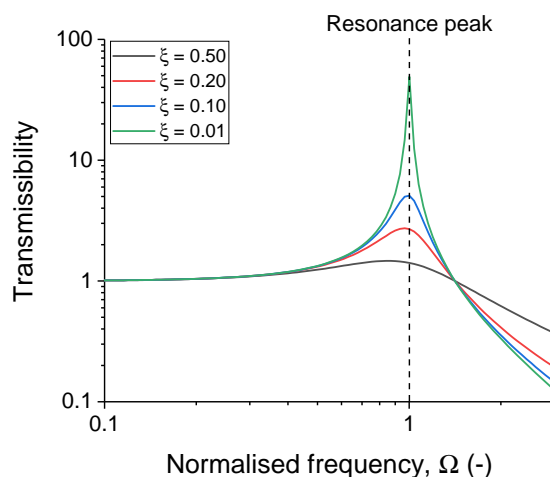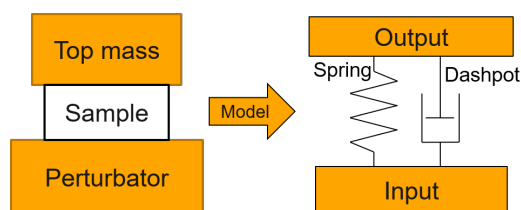ent resonance-based data. The abscissa is often normalised to the natural frequency, which means that the resonance peak occurs when the normalised frequency is equal to 1. In theory, the transmissibility of the resonance peak should increase asymptotically, but is limited by the damping behaviour of the material. In the current investigation, the transmissibility curve will be further investigated with Fourier analysis. [14]

Since this method uses the resonance phenomenon, the experimental setup must be calibrated in terms of sample geometry and added mass, in order to obtain the material resonance in the desired frequency window. The resonance frequency f_o in tension–compression mode can be estimated with the following equation:

$$f_o = \frac{1}{2\pi} \sqrt{\frac{E \cdot S}{l \cdot M}},$$

(2)

where E is the Young's modulus in N/m^2, S is the cross-sectional contact area in m^2, l is the height of the sample in m and M is the added top mass in kg.

The temperature range of operation for the VHF104 is given from -50 to $100\,^\circ$C, however in the present work, only ambient conditions were considered for simplicity. In terms of excitation, the transducer was able to perturbate up to 200 m/s^2. The deformation amplitude was operating in the micrometer range in order to probe the strain-dependent linear viscoelastic region of the rubber sample. In the current setup, tension–compression mode was used due to the geometric simplicity. While it is known that this deformation mode induces nonlinearity due to geometrical effects, the current setup used a small deformation amplitude, hence minimising the aforementioned effect. In addition,

the sample diameter (8 mm) was sufficiently larger than the height (6 mm) of the sample, therefore reducing the risk of transverse bending with respect to the deformation axis.

The material chosen for the investigation was a simple solution-polymerised styrene-butadiene rubber (SSBR) compound with various amounts of carbon black N339 fillers, and is summarised in Table 1.

Table 1. Recipe series used in this study.

Ingredients	Amount (phr) *
SSBR [a]	100.0
N339	0.0–55.0
IPPD [b]	1.5
Zinc Oxide	3.0
Stearic acid	1.0
CBS [c]	2.0
Sulphur	1.4

* Parts per hundred rubber; [a] solution-polymerised styrene-butadiene rubber—styrene content 24%, vinyl content 34%, molecular weight 472.65 kg/mol, Tg $-40\,°C$, PDI 1.65; [b] N-Isopropyl-N′-phenyl-1,4-phenylenediamine; [c] N,N′-Dicyclohexyl-2-benzothiazole sulfenamide.

3. Results and Discussion

3.1. Data Processing

Analog acceleration-time signals were sampled and directly transformed into frequency data using synchronous detection algorithms. For this device, up to three harmonics were observed with significant signal-to-noise ratio with several orders of magnitude. For simplicity, the raw signals will be denoted as input and output signal.

Both the input and output signals were extracted via the built-in option of the standard evaluation software, Dynatest, made for VHF104. The resultant file from each measured frequency f_{expt} contained 512 time-independent points of acceleration amplitude denoted by the incremental value of n, hence a time variable t_n was assigned with the known frequency:

$$t_n = \left(\frac{n}{512}\right)\left(\frac{1}{f_{expt}}\right). \tag{3}$$

These time-domain signals were then transformed into Fourier space, and the result of this procedure is shown in Figure 4. This procedure obeys all three fundamental Fast Fourier Transform (FFT) prerequisites, and therefore the analysis is representative of the real data [14]. The first prerequisite is that the signal was periodic and continuous. Secondly, the sample size was sufficiently large to be representative of the real signal. Finally, the spectral leakage of the signal was minimised by taking values of 2^n. The lowest frequency point (i.e., the first data point) in Figure 4b indicates the first harmonic of the system, which is essentially the main signal used to characterise the viscoelastic behaviour of the material. Apart from spectral leakage, whereby the signal is superficially distorted due to sampling issues from the Fourier transformation, a single peak is expected from a linear or homogeneous system. Evidently, this was not the case as higher harmonics were observed, provided that the frequency range did not exceed the VHF104 excitation limitation of 10 kHz. It should be noted, however, that since the input waveform becomes more erratic as the harmonics increase, only the first three harmonics should be considered for further analysis.

Since the output signal contained residues from the input, normalising the signal gave the theoretical pure signal of the sample. Performing this on each experimental point produced a transmissibility or transfer function curve when plotted against frequency.

$$Transmissibility = \frac{Output\ signal}{Input\ signal} \tag{4}$$

The final outcome of the process is shown in Figure 5. The vibrational modes were defined as the transmissibility of the vibrational harmonics. For example, the intensity-normalised second harmonic of a sample measurement was denoted as the second vibrational mode. Interestingly, all the vibrational modes coincided with one another at certain frequency ranges, which indicates that the first vibrational mode was affecting the subsequent higher-order vibrational modes. Note that the higher vibrational modes were multiple integers of the first vibrational mode. Further discussion will follow in the next section.

(**a**)   (**b**)
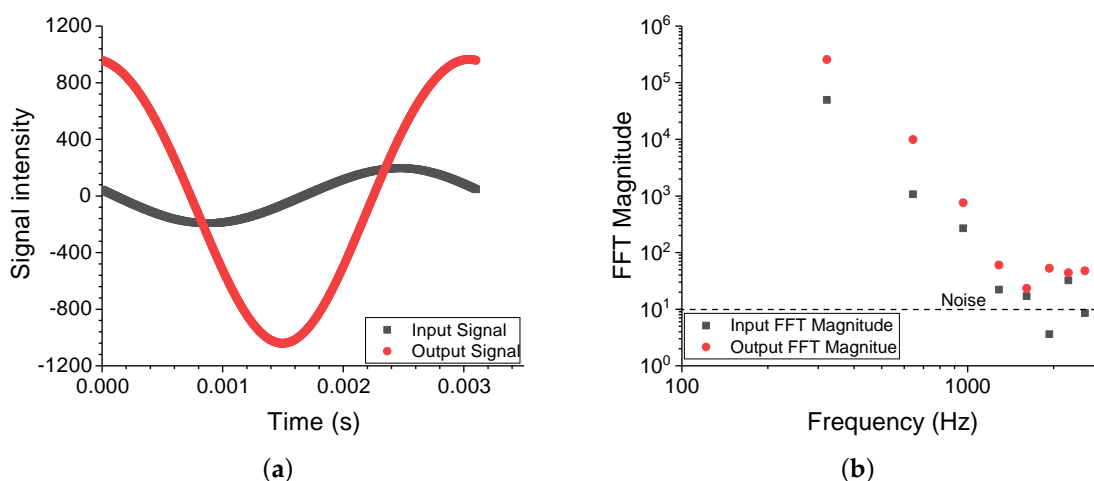
Figure 4. (**a**) Time-domain signal of a 10 phr filled SSBR sample at the resonance frequency of 300 Hz and (**b**) the corresponding Fourier space of the signal. Note that the first three harmonics were several orders of magnitude higher than the background noise.
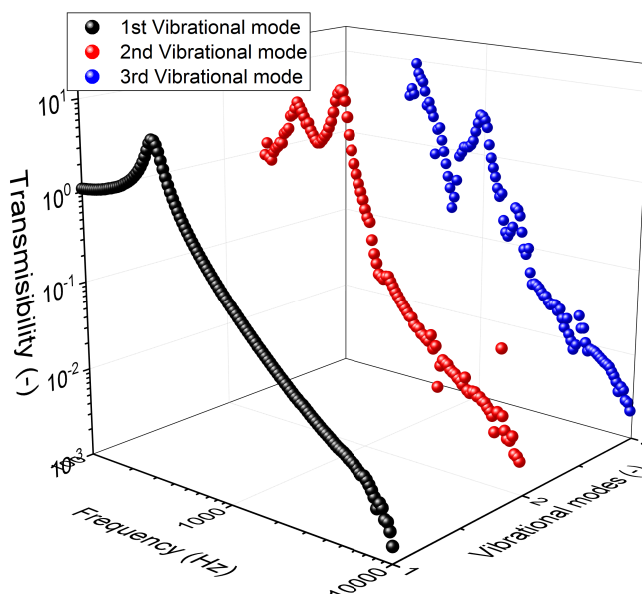
Figure 5. The transmissibility (output normalised to input) curve of the first three vibrational modes.

3.2. Vibrational Superharmonic

The term *vibrational superharmonic resonances* was first quoted by Yang et al. [15] in order to describe the appearance of higher-order resonances seen in nonlinear systems. Their investigation is mostly focused on the frequency response of a bistable system, whereby the system is perturbed with two excitation signals, one being a significantly lower frequency than the other. Nevertheless,

it was noted that a high-frequency perturbation on a nonlinear system can induce both vibrational superharmonic resonance and vibrational subharmonic resonance.

The existence of higher vibrational modes was a unique trait from this experimental setup and could lead to hints on the nonlinearity of the system. In order to probe these higher vibrational modes, a baseline has to be defined as to remove the influence of the prior vibrational mode. In the VHF104, a harmonic vibration was applied at the base of the sample and the so-called reaction mass was bonded at the top of the sample. Assuming a linear system, the equation of motion where the first three terms are defined as the inertia, damping and elastic components of the system is defined as:

$$m\ddot{x} + c(\dot{x} - \dot{x}_e) + k(x - x_{excitation}) = 0. \tag{5}$$

Equation (5) can be further simplified by combining the excitation terms and defining them as an equivalent excitation force, $F_e cos(\omega t)$ with $\omega = 2\pi f$, the pulsation of the applied vibration:

$$m\ddot{x} + c\dot{x} + kx = F_e cos(\omega t). \tag{6}$$

The resultant transmissibility is given in Equation (7) [16], where f is the measured frequency, $f_o = \sqrt{(k/m)}/2\pi$ is the natural frequency of the dynamical system composed of the sample and the reaction mass, and $\xi = c/c_c$ is the damping ratio of the system—essentially the percentage of measured damping with respect to the critical damping, $c_c = 2\sqrt{km}$. As a first approximation, this equation was able to fit the first vibrational mode and was therefore used as a baseline for the subsequent steps.

$$|T_{Linear}| = \frac{F_{transmitted}}{F_{excited}} = \sqrt{\frac{1 + \left(2 \cdot \xi \frac{f}{f_o}\right)^2}{\left(1 - \frac{f^2}{f_o^2}\right)^2 + \left(2 \cdot \xi \frac{f}{f_o}\right)^2}} \tag{7}$$

Normalising the second vibrational mode to the fitted first vibrational mode led to a pure signal response of the mode, as shown in Figure 6. A similar procedure can be done for the third vibrational mode. At this point, the maximum of the normalised vibrational modes were defined as the superharmonic resonances. The normalised second vibrational mode for the selected filler loading is shown in Figure 7.

(**a**)   (**b**)
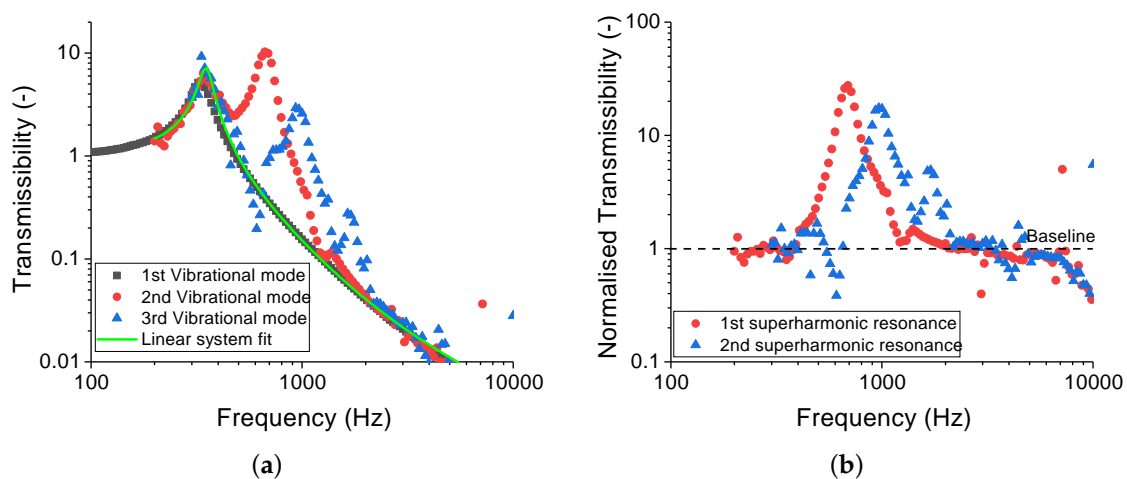
Figure 6. The transmissibility curve for SSBR10CB (**a**) before and (**b**) after normalising to the fitted linear vibration equation. The first superharmonic resonance was defined as the resonance of normalised second vibrational mode.

Taking the amplitude of the superharmonic resonances for all measured samples, the results are plotted in Figure 8a. The second superharmonic resonance had a lower intensity and was more prone to noise as seen in Figure 4b. Therefore, the first superharmonic resonance was the focus of the current investigation. Interestingly, the amplitude of the first superharmonic resonance was a function of the filler amount present in the sample. Its amplitude was reduced with increasing amount of filler, up to the point where the filler percolation threshold ϕ_c occurred. This seems to indicate that the filler was suppressing the intrinsically nonlinear behaviour of the elastomer, up to a point where a filler network was formed ($\phi_c \approx 0.16$ for N339). Beyond this point, the system exhibited a relatively weak nonlinear behaviour, which could be attributed to the aggregation of the filler network. This observation is similar to the maxima observed in elongation at break with the variation of filler amount [17] . At this point, a conclusive statement requires a more thorough investigation as well as the consideration of other possible methods, such as normalising the higher harmonic with the first (see Figure 8b). Such is the case for the Fourier analysis of the rheological test in large-amplitude oscillatory shear (LAOS), whereby the third harmonic is normalised to the first ($I_{3/1}$) [8].
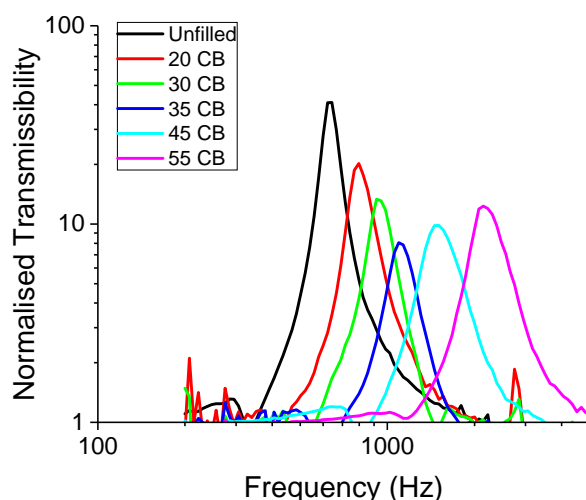

Figure 7. The normalised second vibrational mode as a function of frequency for selected filler loading.
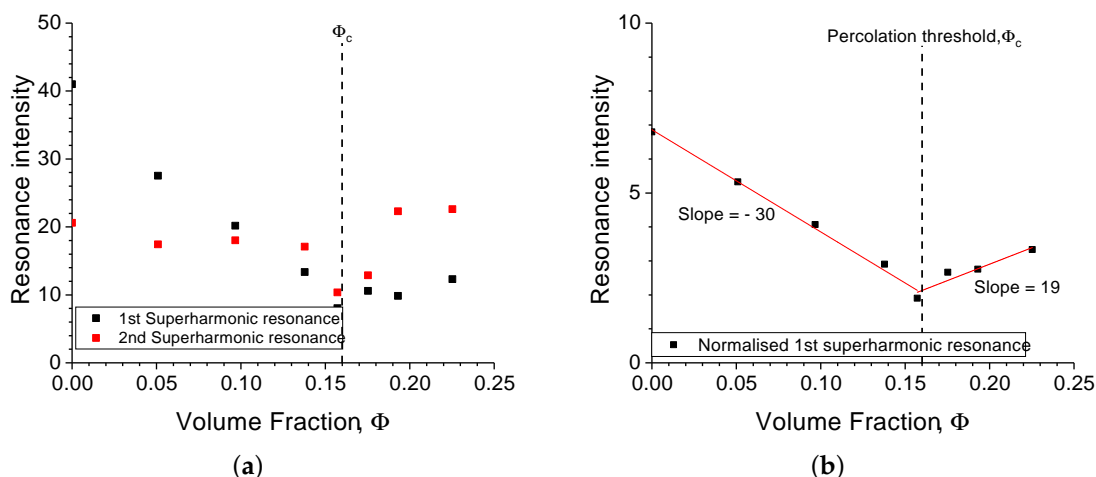

Figure 8. (**a**) The intensity of the first and second superharmonic resonance and (**b**) the intensity of the first superharmonic resonance normalised to the maximum of the first vibrational mode, $I_{2/1}$.

3.3. Foldover Effect

Another consequence of the nonlinear resonance response is the foldover effect, whereby the transmissibility of the resonance is seen to be more asymmetric with respect to the frequency and amplitude of the oscillation. One of the earliest mathematical descriptions of the nonlinear resonance response was made by Landau and Lifschitz, whereby they assumed that the nonlinearity could be described as higher-order terms of the viscous and elastic components of a system [11]. In the present work, only the additional third-order spring term was considered as a first approximation of the foldover effect. Therefore, it was assumed to be a double-potential well system, which is more physically relevant [18]—that is, there was an energetic minimum for the integral of nonlinear spring, $x + x^3$. As a first approximation, the emphasis was placed on the influence of the nonlinearity of the elastic component to characterise the asymmetry of the resonance peak, in analogy to the previous observation in micro-electro-mechanical systems (MEMS) [19].

The first vibrational mode is presented in Figure 9. It can be clearly seen that as the filler amount increased, the resonance peak got progressively more asymmetric. One possible explanation here is that the mechanical response of the filler was vastly different from that of the rubber matrix. Hence, the filler network was not easily deformable as the rubber matrix counterpart. A simple nonlinear response model for a forced oscillation is given in Equation (8). This equation is also known as the Duffing's equation [18].

$$m\ddot{x} + c\dot{x} + k_1 x + k_2 x^3 = F_e cos(\omega t)$$
(8)

The consequence of this equation in terms of transmissibility is given by Equation (9) [20], where $\hat{X}$ is the amplitude of the output signal, α is the cubic nonlinear coefficient, ξ is the damping ratio and Ω ($= f_{expt} / f_{resonance}$) is the resonance-normalised frequency:

$$|T_{Nonlinear}| = \hat{X}\sqrt{(1 + \frac{3}{4}\alpha\hat{X}^2)^2 + 4\xi^2\Omega^2}.$$
(9)

Using the aforementioned formula, the degree of nonlinearity of the material response can be quantified with the α parameter. The influence of the α parameter and the damping factor is depicted in Figure 10. For the linear example, the α parameter was set to a very small value to avoid an undefined solution. Comparing Equations (7) and (9) with a small α parameter values led to the same solution.
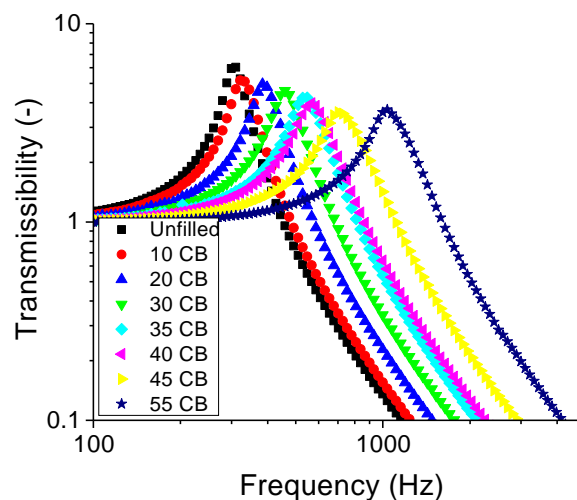

Figure 9. The transmissibility curve of the first vibrational mode with N339 CB.

36

The outcome of the fitting procedure is shown in Figure 11. All of the samples had a fitting tolerance of 4%, which was calculated from the residual ($=|(T_{experiment} - T_{fit})|/T_{experiment}$). The magnitude of the α parameter was observed to increase with higher CB amounts. This means that the filler induced the higher elastic term, and was therefore making the system more nonlinear. Note that only a negative α parameter value was observed, which indicates a softening behaviour. In micro-electro-mechanical systems (MEMS), a similar cubic nonlinearity is also observed but with a positive α parameter, which is referred to as a hardening phenomenon [19].
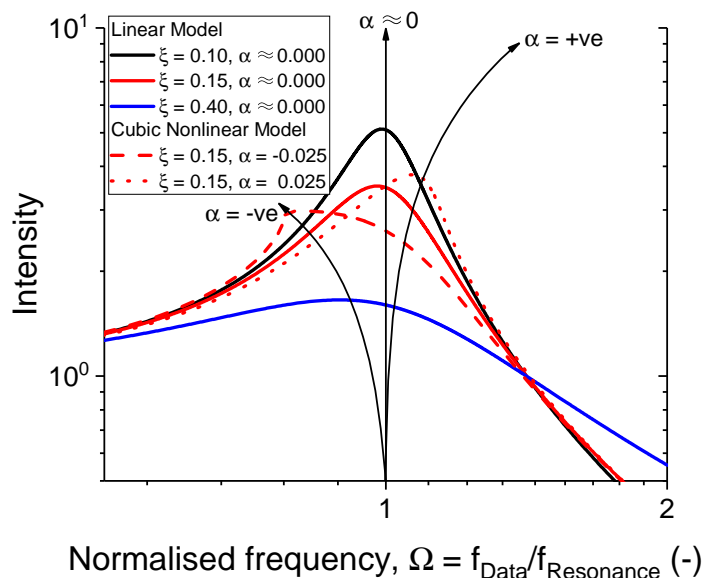

Figure 10. The influence of the cubic nonlinearity coefficient, α-parameter, and the damping factor on the transmissibility curve generated from Equation (9).

The influence of filler amount on the α-parameter values is shown in Figure 12. In contrast to the behaviour of the superharmonic resonance, the α parameter was negligible below the percolation threshold. Its apparent small increase below the percolation threshold was not significant, as it was subjected to the low sensitivity of the first vibrational mode. The α parameter below percolation is to be considered as a numerical artefact obtained by fitting. The increase of the α-parameter was more pronounced beyond the percolation threshold and was in line with the previously observed behaviour of the superharmonic resonance.

Hence, it does seem that the analysis of the superharmonic resonance was the appropriate method of evaluating the nonlinearity since it was able to cover the complete range of filler loading, below and above percolation. While the α parameter is only a fitting parameter for the bending of the transmissibility curve, the superharmonic resonance is a value measured with an excellent signal-to-noise ratio.
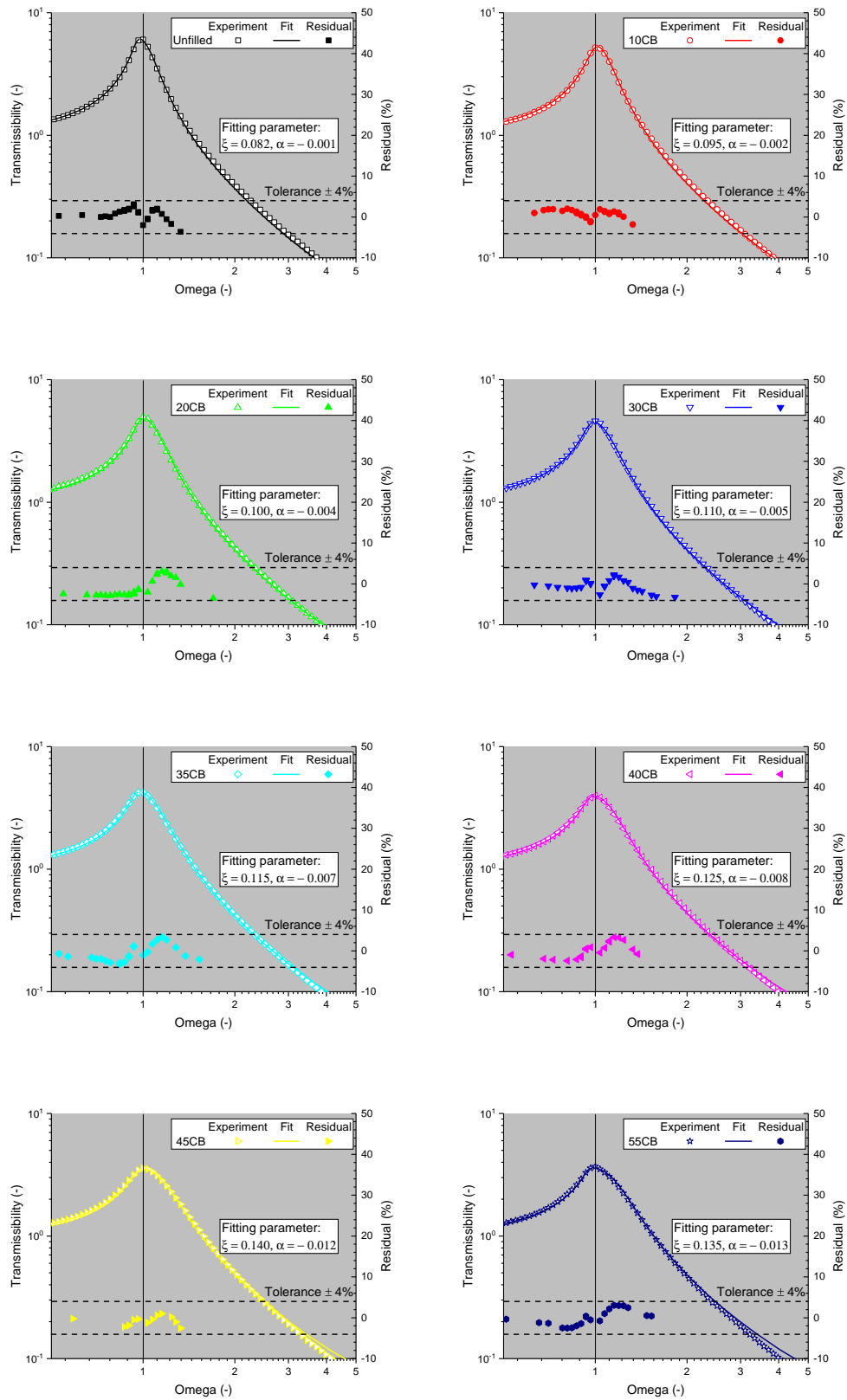
Figure 11. The cubic nonlinearity fit with the corresponding residual values for the current investigation.
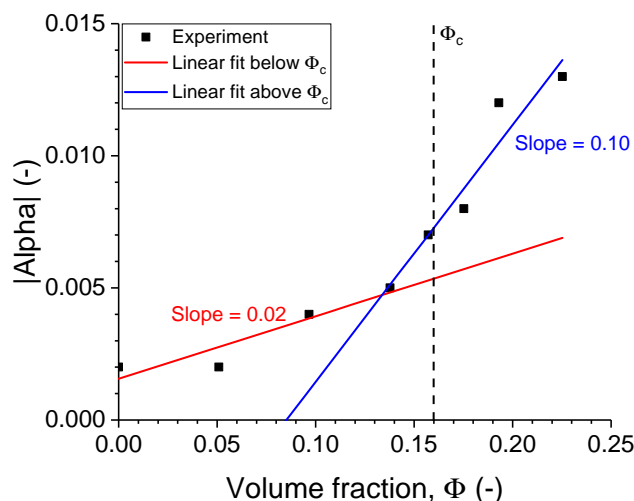
Figure 12. The nonlinear cubic coefficient values for the current investigation. The percolation threshold, ϕ_c, is the value obtained from Figure 8.

4. Conclusions

The nonlinear material response induced by the nanocomposite fillers was analysed by a high-frequency DMA. Firstly, the basis of the device was introduced, as well as the analytical steps for the experimental signal. By transforming the signal into Fourier space, several higher harmonics were observed. Normalising these harmonics with the respective input signal led to vibrational modes that contained superharmonic resonances, which are essentially a harmonic oscillation generated by the nonlinearity of the resonance peak. An apparent correlation was observed between the first superharmonic resonance and the filler amounts, which is a strong indication of filler induced nonlinearity since there seemed to be a crossover point at the percolation threshold ϕ_c. In fact, the resonance peak beyond the percolation threshold exhibited a foldover effect, whereby the resonance peak displayed an asymmetrical behaviour. This behaviour could be described with a nonlinear cubic model with an α parameter that denotes the nonlinearity term. This model, however, is limited to filled compounds which are above the percolation threshold, whereby the filler-induced nonlinearity is dominant. Therefore, the superharmonic resonance seemed to be more sensitive, as both the intrinsic nonlinearity of the elastomer and the filler-induced nonlinearity could be observed. Hence, it is more appropriate to evaluate the nonlinearity based on the superharmonic resonance. Future investigations will involve different filler grades and polymer types so as to give a more universal statement on the current findings.

References

1. Lakes, R.S. *Viscoelastic Solids (Mechanical and Aerospace Engineering Series)*; CRC Press: Boca Raton, FL, USA, 1998.
2. Edwards, S.F.; Vilgis, T.A. The tube model theory of rubber elasticity. *Rep. Prog. Phys.* **1988**, *51*, 243, doi:10.1088/ 0034-4885/51/2/003. [CrossRef]

3. Heinrich, G.; Klüppel, M. Recent Advances in the Theory of Filler Networking in Elastomers. In *Filled Elastomers Drug Delivery Systems*; Springer: Berlin/Heidelberg, Germany, 2002; Chapter 1, pp. 1–44.

4. Payne, A.R. Effect of dispersion on the dynamic properties of filler-loaded rubbers. *J. Appl. Polym. Sci.* **1965**, *9*, 2273–2284, doi:10.1002/app.1965.070090619. [CrossRef]

5. Wilhelm, M.; Reinheimer, P.; Ortseifer, M. High sensitivity Fourier-transform rheology. *Rheol. Acta* **1999**, *38*, 349–356, doi:10.1007/s003970050185. [CrossRef]

6. Ewoldt, R.H.; Winter, P.; Maxey, J.; McKinley, G.H. Large amplitude oscillatory shear of pseudoplastic and elastoviscoplastic materials. *Rheol. Acta* **2010**, *49*, 191–212, doi:10.1007/s00397-009-0403-7. [CrossRef]

7. Ewoldt, R.H.; McKinley, G.H. On secondary loops in LAOS via self-intersection of Lissajous—Bowditch curves. *Rheol. Acta* **2010**, *49*, 213–219, doi:10.1007/s00397-009-0408-2. [CrossRef]

8. Schwab, L. Fourier Transform Rheology of Complex, Filled Rubber Materials. Ph.D. Thesis, Karlsruher Instituts of Technologie, Karlsruhe, Germany, 2016.

9. Schwab, L.; Hojdis, N.; Lacayo, J.; Wilhelm, M. Fourier-Transform Rheology of Unvulcanized, Carbon Black Filled Styrene Butadiene Rubber. *Macromol. Mater. Eng.* **2016**, *301*, 457–468, doi:10.1002/mame.201500356. [CrossRef]

10. Hyun, K.; Wilhelm, M.; Klein, C.O.; Cho, K.S.; Nam, J.G.; Ahn, K.H.; Lee, S.J.; Ewoldt, R.H.; McKinley, G.H. A review of nonlinear oscillatory shear tests: Analysis and application of large amplitude oscillatory shear (LAOS). *Prog. Polym. Sci.* **2011**, *36*, 1697–1753, doi:10.1016/j.progpolymsci.2011.02.002. [CrossRef]

11. Landau, L.D.; Lifshitz, E.M. *Mechanics*; Elsevier Science and Technology: Amsterdam, The Netherlands, 1982.

12. *ASTM D5992-96(2018) Standard Guide for Dynamic Testing of Vulcanized Rubber and Rubber-Like Materials Using Vibratory Methods*; ASTM International: West Conshohocken, PA, USA, 2018. doi:10.1520/D5992-96R18 [CrossRef]

13. Alfrey, T.; Doty, P. The Methods of Specifying the Properties of Viscoelastic Materials. *J. Appl. Phys.* **1945**, *16*, 700–713, doi:10.1063/1.1707524. [CrossRef]

14. Ewins, D.J. *Modal Testing: Theory, Practice, and Application*; Research Studies Press Ltd.: Hertfordshire, UK, 1998.

15. Yang, J.; Sanjuán, M.A.; Liu, H. Vibrational subharmonic and superharmonic resonances. *Commun. Nonlinear Sci. Numer. Simul.* **2016**, *30*, 362–372, doi:10.1016/j.cnsns.2015.07.002. [CrossRef]

16. Lu, Z.; Brennan, M.J.; Chen, L.Q. On the transmissibilities of nonlinear vibration isolation system. *J. Sound Vib.* **2016**, *375*, 28–37, doi:10.1016/j.jsv.2016.04.032. [CrossRef]

17. Bawadukji, N.A.; Jabra, R. Formulation, Preparation, and Mechanical Characterization of Nitrile-Butadiene Rubber (NBR) Composites. *Mater. Sci. Indian J.* **2017**, *15*, 116.

18. von Wagner, U.; Lentz, L. On some aspects of the dynamic behavior of the softening Duffing oscillator under harmonic excitation. *Arch. Appl. Mech.* **2016**, *86*, 1383–1390, doi:10.1007/s00419-016-1123-y. [CrossRef]

19. Budnitzki, M.; Scates, M.; Ritchie, R.; Stach, E.; Muhlstein, C.; Pierron, O. The effects of cubic stiffness on fatigue characterization resonator performance. *Sens. Actuators A Phys.* **2010**, *157*, 228–234. [CrossRef]

20. Carrella, A.; Brennan, M.; Waters, T. Force transmissibility of a nonlinear vibration isolator with high-static-low-dynamic stiffness. In Proceedings of the 6th EUROMECH Nonlinear Dynamics Conference, Saint Petersburg, Russia, 30 June–4 July 2008.

4.3 Superharmonic resonance in carbon black filled rubber by High-Frequency DMA

The final paper [52] is meant to bind the first two papers together. The superharmonic resonance method described in the previous paper was used to investigate the resin impact on the the filler network. The paper is separated into 3 sections.

In the first section, a prefactor is introduced to the superharmonic resonance data in order to compensate the various displacement excitations that the sample undergoes. This new term is called the normalised superharmonic resonance, nSHR.

In the following section, three systematic studies of carbon black grades N121, N339 and N550 of various concentrations were analysed. It was concluded that the onset of the percolation threshold, which was measured independently with the RPA, did indeed affect the nonlinearity of the compound. However, when coupled with TEM images, the filler dispersion within the rubber matrix also plays a large role in the material nonlinearity. A well percolated network would result in a highly nonlinear response due to the pronounced stress gradient between the filler network and polymer system.

The final section revisits the first paper, whereby the reinforcing resin is seen to modify the surface of the carbon blacks, which in turn affect the filler network morphology. The increase of reinforcing resin concentration makes the filler network more compact, and thus, introduces higher nonlinearity to the sample.

Superharmonic Resonance in Carbon-Black-Filled Rubber by High-Frequency DMA

Imran Hussain Syed * [ID] **and Jorge Lacayo-Pineda**

Continental Reifen Deutschland GmbH, Jaedekamp 30, 30419 Hannover, Germany; jorge.lacayo-pineda@conti.de
* Correspondence: imran.syed@conti.de

Abstract: A systematic study of several SBR compounds filled with carbon black of various grades were analysed with the high-frequency Dynamic Mechanical Analyzer (HF DMA) in order to quantify the degree of nonlinearity induced by fillers in rubber compounds. These filler grades indirectly reflect different degrees of microdispersion, which seems to be the main influence on the superharmonic resonance phenomenon observed in HF DMA. This statement arises from the comparison of the microdispersion observed in TEM images. In the second part of the paper, a model compound filled with carbon black is enhanced with a standard reinforcing resin, which leads to a more compact filler network. This induces a higher superharmonic resonance response as well as a higher transmissibility behaviour.

Keywords: nonlinearity; superharmonic resonance; HF DMA

1. Introduction

Fillers are introduced into rubber compounds to improve their mechanical properties such as elongation at break, shore hardness, and abrasion [1–3]. It is known from Fourier Transform (FT) rheology that carbon black enhances the nonlinear mechanical behaviour of the compound. The nonlinearity here is referring to the appearance of higher harmonics within the DMA response signal for a sample that is under defined deformation conditions. Nonlinearity is known to be quantified by the ratio of the third to the first harmonic amplitude, I(3/1) in FT Rheology [4–8]. While FT rheology is a strain dependent analysis of the Fourier response, the high-frequency Dynamic Mechanical Analyzer (HF DMA) allows for a resonance-based, frequency dependent analysis of the Fourier response. The outcome of this frequency analysis is the appearance of the vibrational superharmonic resonance.

Vibrational resonance was first reported by Landa and McClintock [9] in order to describe a nonlinear signal response which is weakly perturbed by a secondary, significantly weaker oscillator into the system. Following this work, Yang et al. [10] observed higher resonance response from the same system. In order to describe this behaviour, the terms vibrational superharmonic resonance (VsupR) and vibrational subharmonic resonance (VsubR) were proposed to represent the presence of higher-order and lower-order resonances, respectively.

In the previous investigation, a superharmonic resonance phenomenon was observed in rubber compounds using the Fourier analysis of the resonance peak from HF DMA [11]. There exists a transition between polymer-related nonlinearity and filler-induced nonlinearity. This transition coincides with the percolation threshold of the filler network and gives a hint on the origins of the observed superharmonic resonance. The present work is aimed at elucidating the correlation between the filler network and the superharmonic resonance.

In another investigation, it was concluded that novolac-type phenolic resin changes the interfacial properties of the carbon black (CB) filler network [12]. This was concluded based on thermomechanical as well as microscopical measurements on filled isoprene rubber compounds with various resin concentrations. The reinforcing resin reduces the percolation threshold of filled compounds by creating interfaces between the carbon black aggregates.

The current investigation is divided into two parts; the influence of polymer types and carbon black grades, and the influence of reinforcing resins. In the first part, an isoprene rubber (IR) filled with N339 carbon black is compared with a solution-polymerized styrene-butadiene rubber (SSBR)-type of the same filler grade. Then, using the SSBR compound as a base, three different filler grades, N121, N339, and N550 are used to compare the filler grade influence on the superharmonic resonance. The second part of the paper aims to further elucidate the superharmonic resonance by introducing reinforcing resin which has been proven to reduce the percolation threshold by modifying the carbon black interfaces.

2. Materials and Methods

The main tool for this investigation is the high-frequency DMA, VHF104 by Metravib, Lyon, France. The general concept of the device is the measurement of the resonance peak on a system comprising of the sample and two metal cylinders; one acting as the excitation base and the other as the preload force onto the sample. The fundamental advantage of this device is the ability to directly measure the mechanical response of a material up to 10 kHz, as opposed to other traditional DMA devices which typically have a maximum frequency of 100 Hz. In terms of absolute deformation amplitude, the latter can achieve values of 9 mm at low frequencies (e.g., DMA Gabo Eplexor 2000N$^{®}$, Netzsch, Alhden, Germany), while the high-frequency DMA is able to reach values of around 300 μm. This value however is highly dependent on the applied top mass of the system.

This DMA is a type of forced vibration resonant system [13], which indicates that the experimental setup must be calibrated in terms of sample geometry and added mass in order to obtain the material resonance in the desired frequency window. The resonance frequency f_o in tension–compression mode can be estimated with the following equation:

$$f_o = \frac{1}{2\pi}\sqrt{\frac{E \cdot S}{l \cdot M}},$$ (1)

where E is the Young's modulus in N/m^2, S is the cross-sectional contact area in m^2, l is the height of the sample in m, and M is the added top mass in kg.

The VHF104 is able to operate at temperature ranges between -50 °C to 100 °C, however, the focus of the present work will be limited to ambient conditions. The excitation displacement was set to 0.1 mm, however, when the value cannot be achieved after certain frequencies, a maximum excitation acceleration of 200 mm/s^2 is used instead due to the limitations of the oscillator acting on the excitation base. Therefore, a correction procedure is applied in the evaluation in the next section. Finally, the tension–compression deformation modes were selected due to the relative simplicity of the sample geometry.

For an independent determination of the percolation threshold, dynamic strain-dependent measurements were performed on the Rubber Process Analyzer RPA 2000 by Alpha Technologies, Hudson, NY, USA. The applied strain amplitudes were chosen from 0.3% up to 100% at 70 °C.

The transmission electron microscopy (TEM) analysis was performed on a JEM1400 Instrument (Jeol, Tokyo, Japan) using a voltage of 100 kV. In order to investigate the CB network structure, samples were measured in the bulk state. Thin slices of approximately 60 nm were prepared by using a cryo-ultramicrotome (Leica EM UC6/EM FC6) equipped with a diamond knife.

The samples chosen for the investigation are solution-polymerized styrene-butadiene rubber (SSBR) compounds with three different grades of carbon black; N121, N339, and N550, at various concentration levels. Additionally, isoprene rubber (IR) compounds with various

concentrations of CB N339 and reinforcing resin were investigated. These recipes are summarised in Tables 1 and 2, respectively.

Table 1. Recipe for the carbon-black-type series used in this study (all values in parts per hundred rubber).

Ingredients	N121	N339	N550
SSBR [a]	100.0	100.0	100.0
Filler	0.0–55.0	0.0–55.0	0.0–75.0
IPPD [b]	1.5	1.5	1.5
Zinc Oxide	3.0	3.0	3.0
Stearic Acid	1.0	1.0	1.0
CBS [c]	2.0	2.0	2.0
Sulphur	1.4	1.4	1.4

[a] Microstructure: styrene content 24%, Vinyl content 34%, molecular weight 472.65 kg/mol, Tg = −40 °C.
[b] N-isopropyl-N′-phenyl-1,4-phenylenediamine. [c] N-cyclohexyl-2-benzothiazole sulfenamide.

Table 2. Recipe for the reinforcing resin series used in this study (all values in parts per hundred rubber).

Ingredients	Reinforcing Resin
IR [d]	100.0
N339	20.0–60.0
Resorcinol	0.0/0.7/4.6
HMMM [e]	0.0/0.7/4.6
6PPD [f]	2.0
TMQ [g]	1.0
Zinc Oxide	6.0
Stearic Acid	1.0
Processing Oil	3.0
DCBS [h]	1.0
Sulphur	4.0

[d] Microstructure: 97% cis, molecular weight 1300 kg/mol, Tg = −65 °C. [e] hexamethoxymethyl-melamine.
[f] N-(1,3-dimethylbutyl)-N′-phenyl-p-phenylene diamine. [g] 2,2,4-trimethyl-1,2-dihydroquinoline. [h] N,N′-dicyclohexyl-2-benzothiazole sulfenamide.

3. Results and Discussion

3.1. The Superharmonic Resonance

The analytical approach for the extraction of superharmonic resonance values has been discussed elsewhere [11]. The first vibrational mode is fitted with the linear transmissibility formula, which is then used to normalise the 2nd vibrational mode. The resonance peak of the normalised 2nd vibrational mode is defined as the 1st superharmonic resonance. In the current investigation, the term is simplified to superharmonic resonance since higher superharmonic resonances are more prone to measurement noise.

In the same investigation, the amount of N339 carbon black was varied in SSBR and measured with HF DMA. Two distinct nonlinearities were observed; the nonlinearity originating from the polymer, and the filler-induced nonlinearity. Above the percolation threshold, the latter becomes more dominant than the former. In the aforementioned investigation, the applied strain was assumed to be constant throughout the measurement range. This assumption was sufficient within the experimental setup as to understand the nonlinear behaviour observed. Increasing the level of compound complexity requires a more rigorous consideration of the strains.

When considering different compounds, it is important to note that the excitation input of the experiment is a function of both amplitude and frequency. There is, however, an instrumental limitation on the excitation since a substantial amount of power would be required to have a large amplitude at higher frequencies. As shown in Figure 1, the displacement excitation is reduced at higher frequency

ranges. When the desired excitation amplitude cannot be achieved, a constant base acceleration of 200 m/s^2 is used. The drop in amplitude with respect to frequency can be formulated as follows:

$$Excitation\ displacement, x_{input} = 10^{0.7} \cdot frequency_{input}^{-2}. \tag{2}$$
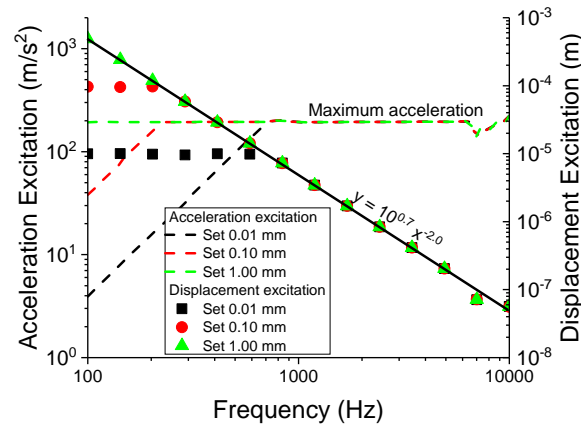

Figure 1. The excitation relation between the displacement and acceleration.

Since the resonance frequency f_o is shifted due to the difference in sample modulus, the sample does not experience the same level of excitation. This can be accounted for by using f_o as a prefactor for the subsequent normalised superharmonic resonance (nSHR). Hence, for simplicity, a new term is introduced to accommodate both the superharmonic resonance as well as the aforementioned corrections:

$$normalised\ superharmonic\ resonance, nSHR = \frac{(f_o)(1st\ superharmonic\ resonance)}{resonance\ amplitude}. \tag{3}$$

The nSHR values between SBR-filled compounds and IR-filled compounds are shown in Figure 2. Above the percolation threshold, the slopes of nSHR for both polymer compounds are similar, and henceforth, indicates a similar filler-induced nonlinearity of the CB. Below the percolation threshold however, the gradient is different, hence, an indication of a polymer-dependent nonlinear response.
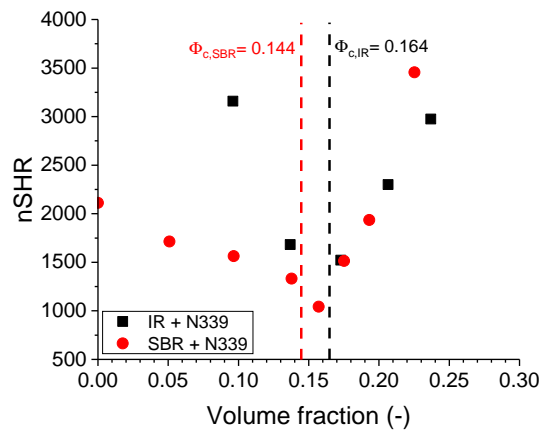

Figure 2. The normalised superharmonic resonance for carbon black (CB)-filled styrene-butadiene rubber (SBR) and isoprene rubber (IR) compounds. The percolation thresholds were obtained by Rubber Process Analyzer (RPA).

3.2. Carbon Black Grades

The three variants of CB grades are known to have different filler structure and size. It is also known that the CB structure plays an important role in the nonlinearity of the compound within FT Rheology [14]. Therefore, a similar approach is used in the present work to decouple the filler influence and the polymer matrix response.

When comparing the resonance frequency in HF DMA with respect to the CB volume fraction, as shown in Figure 3, the onset of the filler network reinforcement as indicated by the percolation threshold can be estimated in analogy to the RPA whereby the deviation of the hydrodynamic reinforcement of the sample determines the percolation threshold. It should be noted from Equation (1) that the resonance frequency is a function of both modulus and geometry. Nevertheless, when comparing the same geometry, the resonance frequency shows a similar strain dependency with respect to CB volume fractions, such is the case for the dynamic strain sweep measurements from the RPA.
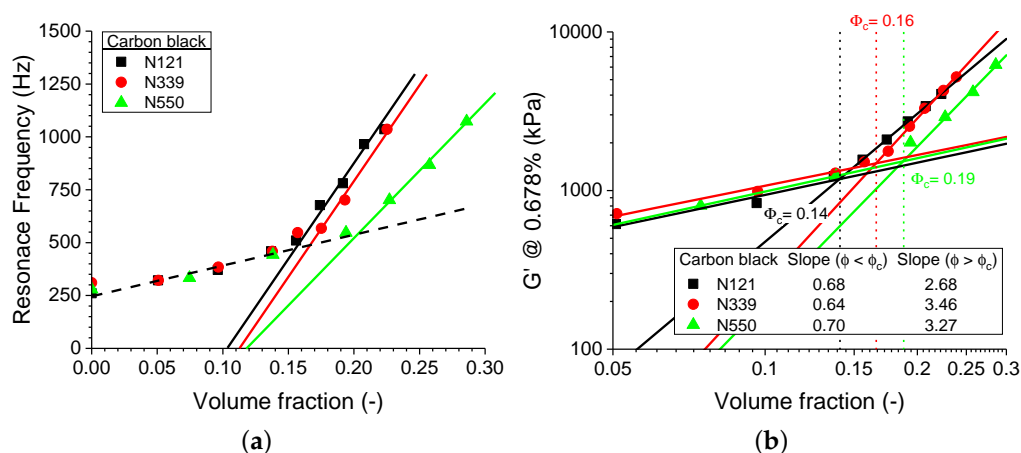

Figure 3. The (**a**) resonance frequency and (**b**) the corresponding storage modulus at low strain of the solution-polymerized styrene-butadiene rubber (SSBR) compounds, as described in Table 1. The dotted lines in (**b**) indicate the corresponding percolation thresholds obtained by RPA measurements.

The normalised superharmonic resonance as a function of CB volume fraction is shown in Figure 4. Similar to Figure 3, the onset at the percolation threshold can be observed. For N121 and N339 compounds, the nSHR value as an indicator of nonlinearity shows a similar CB volume fraction dependency, while the N550 compound shows a much weaker dependency. One plausible explanation of this behaviour is the relatively poor microdispersion of N550 present in the rubber matrix. Images from TEM in Figure 5 seem to justify the hypothesis, especially when compared to the other two carbon black grades. It is possible that the filler particles are scattering the mechanical wave propagation through the sample from the input to the output sensor. Above the percolation threshold however, a secondary wave propagation is induced by the filler structure due to the large modulus difference between the viscoelastic matrix and the filler network. This implies that the slope of nSHR might be an indication of filler distribution within the compound.

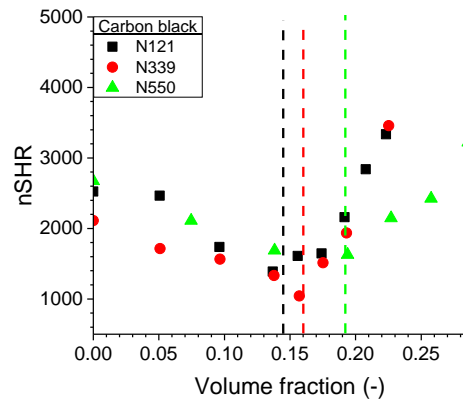**Figure 4.** The normalised superharmonic resonance (nSHR) values for three carbon black grades; N121, N339, and N550 within a SSBR matrix. The dashed vertical lines represent the percolation threshold obtained by RPA for each compound.
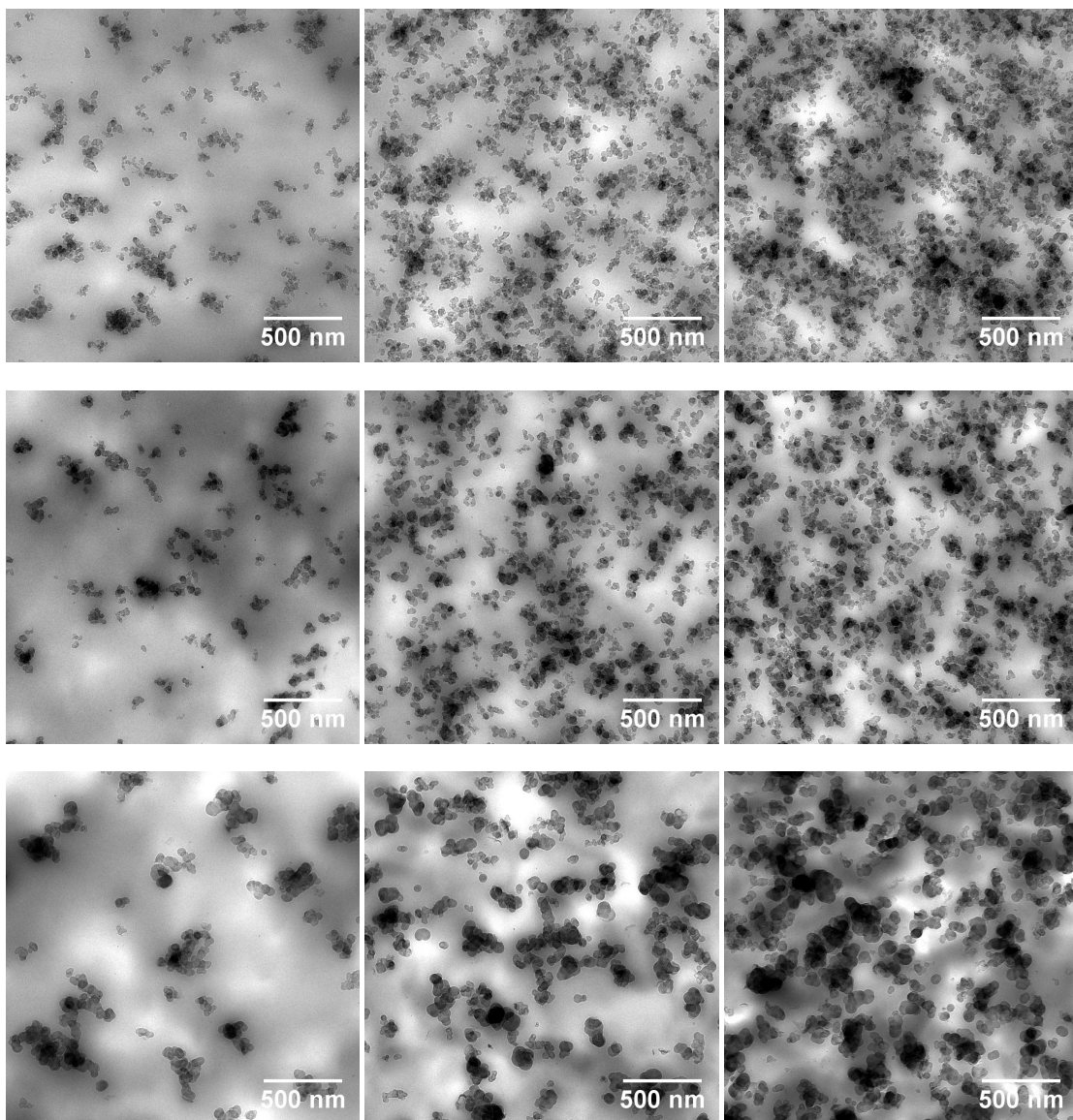

Figure 5. TEM images for N121 (**top row**), N339 (**middle row**), and N550 (**bottom row**) in SSBR compounds with filler concentrations below, around, and above percolation threshold.

47

3.3. Reinforcing Resin

In the previous investigation, it was concluded that novolac-type phenolic resin changes the interfacial properties of the CB filler network [12]. This resin-mediated filler network enhances the mechanical properties of the material. This was inferred when the percolation threshold of the polymer was reduced with the introduction of resin as well as the higher mechanical softening behaviour with respect to the applied strain deformation and temperature dependency. Therefore, the filler-induced nonlinearity should be affected by the modification of the filler network interphase by resin.

The resonance amplitude is inversely proportional to the damping coefficient. Looking at the resonance amplitude of the first vibrational mode in Figure 6b, the damping coefficient is seen to be reduced for the compound with substantial amount of resin. This means that the polymer has a stronger elastic behaviour with a higher amount of filler and resin combinations. This behaviour was not observed in the aforementioned CB variation studies, as indicated in Figure 6a. In other words, the resin-mediated compounds are able to channel the mechanical wave more effectively through the sample without heavy signal attenuation.
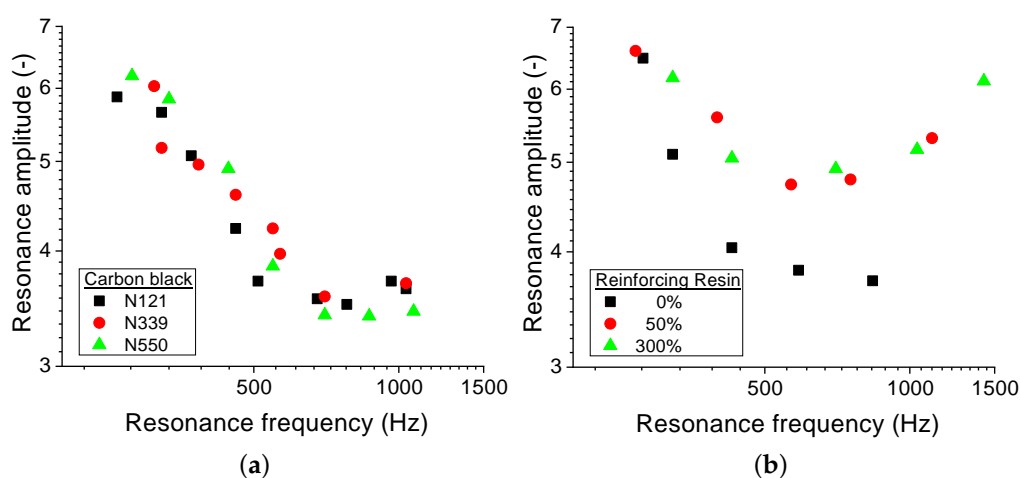
Figure 6. The resonance amplitude as a function of resonance frequency for (**a**) different carbon black grades within a SSBR matrix without resin and (**b**) carbon-black-filled IR with three resin concentrations; 0.0, 1.4, and 9.2 parts per hundred rubber.

Observing the normalised superharmonic resonance (nSHR) values in Figure 7, the nonlinearity of the resin compound is significantly higher than the nonresin analogue. Utilising the conclusion from the previous studies, the nonlinearity induced by the filler network is enhanced by the resin and is attributed to a more compact network formed in the polymer.

Figure 7. The nSHR values for the three resin concentrations in a N339-filled IR compound. Dashed lines indicate percolation threshold values obtained by RPA measurements. Note that the scaling is twice the scale in Figure 4.
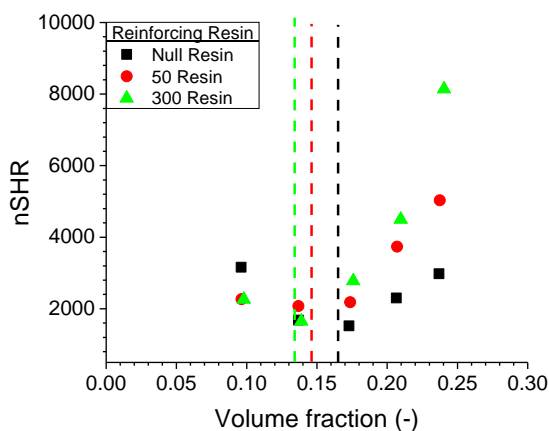
4. Conclusions

A systematic study of three variants of SBR matrix filled with either N121, N339, or N550 carbon black grades was performed in order to elaborate the superharmonic resonance effects in terms of filler volume fractions. The filler-induced nonlinearity in the N550 compound is much weaker than the other two counterparts, indicating that the microdispersion of the filler plays a role in the superharmonic resonance effects, as validated by TEM images. Following this, reinforcing resin was introduced in an IR matrix in order to investigate the effects of a compact filler network. The compactness of the filler network leads to the compounds with high resin content to exhibit a significantly high normalised superharmonic resonance, further consolidating the hypothesis that the filler network is indeed inducing a secondary mechanical propagation wave which leads to the nonlinearity effects of filled compounds.

References

1. Vilgis, T.A.; Heinrich, G.; Klueppel, M. *Reinforcement of Polymer Nano-Composites: Theory, Experiments and Applications*; Cambridge University Press: Cambridge, UK, 2009. [CrossRef]
2. Heinrich, G.; Klüppel, M. Recent Advances in Polymer Science. In *Filled Elastomers: Drug Delivery Systems*; Springer: Berlin/Heidelberg, Germany, 2002; Volume 160, pp. 1–44.
3. Payne, A.R. Effect of dispersion on the dynamic properties of filler-loaded rubbers. *J. Appl. Polym. Sci.* **1965**, *9*, 2273–2284. [CrossRef]
4. Schwab, L. Fourier Transform Rheology of Complex, Filled Rubber Materials. Ph.D. Thesis, Karlsruher Institute of Technology, Karlsruhe, Germany, 2016.
5. Ewoldt, R.H.; Winter, P.; Maxey, J.; McKinley, G.H. Large amplitude oscillatory shear of pseudoplastic and elastoviscoplastic materials. *Rheol. Acta* **2010**, *49*, 191–212. [CrossRef]
6. Ewoldt, R.H.; McKinley, G.H. On secondary loops in LAOS via self-intersection of Lissajous—Bowditch curves. *Rheol. Acta* **2010**, *49*, 213–219. [CrossRef]

7.　Wilhelm, M.; Reinheimer, P.; Ortseifer, M. High sensitivity Fourier-transform rheology. *Rheol. Acta* **1999**, *38*, 349–356. [CrossRef]

8.　Hyun, K.; Wilhelm, M.; Klein, C.O.; Cho, K.S.; Nam, J.G.; Ahn, K.H.; Lee, S.J.; Ewoldt, R.H.; McKinley, G.H. A review of nonlinear oscillatory shear tests: Analysis and application of large amplitude oscillatory shear (LAOS). *Prog. Polym. Sci.* **2011**, *36*, 1697–1753. [CrossRef]

9.　Landa, P.S.; McClintock, P.V.E. Vibrational resonance. *J. Phys. A Math. Gen.* **2000**, *33*, 433–438. [CrossRef]

10.　Yang, J.; Sanjuán, M.A.; Liu, H. Vibrational subharmonic and superharmonic resonances. *Commun. Nonlinear Sci. Numer. Simul.* **2016**, *30*, 362–372. [CrossRef]

11.　Syed, I.; Vouagner, P.; Fleck, F.; Lacayo-Pineda, J. Nonlinearity in the Mechanical Response of Rubber as Investigated by High-Frequency DMA. *Polymers* **2019**, *11*, 581. [CrossRef] [PubMed]

12.　Syed, I.; Klat, D.; Braer, A.; Fleck, F.; Lacayo-Pineda, J. Characterizing the influence of reinforcing resin on the structure and the mechanical response of filled isoprene rubber. *Soft Mater.* **2018**, *16*, 275–288. [CrossRef]

13.　*ASTM D5992-96(2018) Standard Guide for Dynamic Testing of Vulcanized Rubber and Rubber-Like Materials Using Vibratory Methods*; ASTM International: West Conshohocken, PA, USA, 2018. [CrossRef]

14.　Schwab, L.; Hojdis, N.; Lacayo, J.; Wilhelm, M. Fourier-Transform Rheology of Unvulcanized, Carbon Black Filled Styrene Butadiene Rubber. *Macromol. Mater. Eng.* **2016**, *301*, 457–468. [CrossRef]

Chapter 5

Summary and Outlook

5.1 Summary

The present work introduces various novel methods of characterising filler network in rubber compound. The most significant finding is the observation of the superharmonic phenomenon in rubber compounds for the first time. More commonly seen in micro-electro-mechanical systems (MEMS) such as accelerometers and gyroscopes, the superharmonic resonance in rubber is seen to be mainly affected by the filler network and microdispersion. Therefore, any modifications to the filler network would be reflected in the rheologically nonlinear, non-sinusoidal mechanical response of the compound. This statement is derived from the following peer-reviewed publications.

In the first publication, the effects of resorcinol-based reinforcing resin on the carbon black filler network is investigated via various experimental approaches. From the cyclic tensile tests, it was shown that a percolated filler network is required in order to observe the reinforcing effects of the resins. With dynamic mechanical experiments, it was concluded that the percolation threshold is reduced with the addition of reinforcing resin, and the filler network interphase exhibits a higher temperature sensitivity with the addition of resins. TSSR measurements were then performed to validate the impact of reinforcing resin on a higher magnitude, both in terms of the temperature and strain dependency. These results are inline with the previous mechanical experiments. Finally, microscopical techniques were able to validate the compactness of the filler network via the resin mediated networks.

The second published article introduces a novel technique of analyzing the Fourier space of a resonance-based DMA measurement. The input and output signals of the HF DMA measurement are transformed into Fourier space and normalized to obtain a transmissibility curve of the mechanical response of the compound. The outcome of this procedure is the observation of the superharmonic resonance, which is connected to the nonlinearity induced by the presence of fillers within a rubber compound. This was concluded from the systematic study of filler loading which coincides with the percolation threshold obtained by an independent DMA method. In addition, a Duffing's nonlinear cubic model based on the Kelvin-Voigt visco-elastic model, was used to quantify the apparent

foldover effect observed in the transmissibility curve of the measurements. The fitted nonlinear elastic term α in the Duffing's model, seems to correlate with the observed superharmonic resonance since a different filler concentration dependency is obtained below and above the filler percolation threshold.

Finally, the third paper utilizes the analytical technique introduced in the second paper to evaluate the impact of polymer types, filler types and reinforcing resin concentration on the superharmonic resonance. Below the percolation threshold, a polymer dependent nonlinearity is observed while above the percolation threshold, the micro-dispersion of carbon black dominates the nonlinearity behavior. This was further consolidated with the addition of reinforcing resin, whereby the degree of nonlinearity is further increased due to the existence of a resin mediated filler network. In addition, a pre-factor was introduced in the quantification of the superharmonic resonance to take into account the excitation amplitude differences imposed on the sample. It was noted here that the excitation amplitude is a function of the applied frequency.

The current investigation was all performed at ambient temperature in order to simplify the design of experiment. Extending the understanding of the superharmonic resonance in rubber compounds, a more extensive study of the temperature dependency should be performed. Since the mechanical response of rubber compounds is based on the glass transition temperature, this infers that the nonlinearity behavior of rubber would have a significant impact on the measured superharmonic resonance.

Additionally, the Duffing's model was briefly used to describe the rheologically nonlinear response seen within the transmissibility curve of filled rubber compounds above the percolation threshold. The fundamental assumption of the model is that the nonlinearity is originating from the higher orders of the elastic term of the Kevin-Voigt system. The model could be further developed with a higher ordered damping term, in order to derive a more precise material description.

Finally, additional material aspects should be considered in future investigations. In the present work, carbon blacks of different grades and concentrations coupled with reinforcing resin were investigated. More complex compounds, such as silica filled rubber, would be an interesting research topic due to the different reinforcing mechanism. The former having a physically adsorbed interface with the rubber matrix and the latter through a covalent bonds created via the addition of silanes. Softeners would be another interesting topic as they change the polymer chain mobility, and thus, would impart an influence on the apparent polymer induced nonlinearity observed in the superharmonic resonances.

Resume

Personal Information

Name:	Syed Imran Hussain Syed Javaid Iqbal
Date of Birth:	01.06.1987
Place of Birth:	Kedah, Malaysia
Nationality:	Malaysian
Marital Status:	Married

Educational

from 2016	PhD Candidate Gottfried Wilhelm Leibniz Universität Hannover, Germany
2012 - 2015	Master of Science in Polymer Material Science Martin Luther Universität Halle-Wittenberg, Germany
2008 - 2012	Bachelor of Science (Hons) in Physics University Tunku Abdul Rahman, Malaysia
2007 - 2008	Foundation in Science Programme University Tunku Abdul Rahman, Malaysia
2005 - 2007	Cambridge A-level (Science) Tunku Abdul Rahman College, Malaysia
2000 - 2004	Secondary School SMK Taman Bukit Maluri, Malaysia
1994 - 1999	Primary School SK Menjalara, Malaysia

Publications

2019	Superharmonic Resonance in Carbon-Black-Filled Rubber by High-Frequency DMA
2019	Nonlinearity in the Mechanical Response of Rubber as Investigated by High-Frequency DMA
2018	Characterizing the influence of reinforcing resin on the structure and the mechanical response of filled isoprene rubber
2016	Entanglements, defects, and inhomogeneities in nitrile butadiene rubbers: Macroscopic versus microscopic properties

Bibliography

[1] C. Slack. Noble Obsession: Charles Goodyear, Thomas Hancock, and the Race to Unlock the Greatest Industrial Secret of the Nineteenth Century. Hyperion Books, 2002. ISBN 9780786867899.

[2] E. Ehabe, G.E. Nkeng, and F. Bonfils. Mechanistic proposals for variations in the macrostructure of natural rubber. a review. Recent Res. Dev. Bioener, 4(8):l–107, 2006.

[3] Fritz Ullmann, editor. Ullmann's Encyclopedia of Industrial Chemistry. Wiley-VCH, Weinheim, 2006. ISBN 3527313184.

[4] J.B. Donnet. Carbon Black: Science and Technology, Second Edition. Taylor & Francis, 1993. ISBN 9780824789756.

[5] J.E. Mark, B.R. Erman, and M. Roland. The science and technology of rubber. Elsevier BV, 2013. doi: 10.1016/C2011-0-05820-9.

[6] V. Nigam, Dipak Setua, and G. Mathur. Hybrid filler system for nitrile rubber vulcanizates. Journal of Materials Science, 36:43–47, 2001. doi: 10.1023/A:1004874305070.

[7] K. Hyun, M. Wilhelm, C.O. Klein, K.S. Cho, J.G. Nam, K.H. Ahn, S.J. Lee, R.H. Ewoldt, and G.H. McKinley. A review of nonlinear oscillatory shear tests: Analysis and application of large amplitude oscillatory shear (LAOS). Progress in Polymer Science, 36(12):1697–1753, 2011. doi: 10.1016/j.progpolymsci.2011.02.002.

[8] ASTM D8363 Standard Test Method for Rubber—Stress Relaxation in Tension Under Non-Isothermal Conditions, volume 09.01. ASTM International, West Conshohocken, 2020. doi: 10.1520/D8363-20.

[9] Utz von Wagner and Lukas Lentz. On some aspects of the dynamic behavior of the softening duffing oscillator under harmonic excitation. Archive of Applied Mechanics, 86(8):1383–1390, 2016. doi: 10.1007/s00419-016-1123-y.

[10] R. Mülhaupt. Hermann staudinger and the origin of macromolecular chemistry. Angewandte Chemie International Edition, 43(9):1054–1063, 2004. doi: 10.1002/anie.200330070.

[11] J.C. Jansen. Glass Transition Temperature (Tg), pages 1–3. Springer Berlin Heidelberg, Berlin, Heidelberg, 2016. ISBN 978-3-642-40872-4. doi: 10.1007/978-3-642-40872-4_267-1.

[12] M. Rubinstein and R.H. Colby. Polymer Physics. OUP Oxford, 2003. ISBN 9780198520597.

[13] O. Onokpise and C. Louime. The potential of the south american leaf blight as a biological agent. Sustainability, 4(11):3151–3157, 2012. doi: 10.3390/su4113151.

[14] C. L. Swanson, R. A. Buchanan, and F. H. Otey. Molecular weights of natural rubbers from selected temperate zone plants. Journal of Applied Polymer Science, 23(3):743–748, 1979. doi: 10.1002/app.1979.070230309.

[15] V. Vishwanath and H.M. Rao. Gutta-percha in endodontics-a comprehensive review of material science. Journal of conservative dentistry: JCD, 22(3):216, 2019.

[16] X. Men, F. Wang, G.-Q. Chen, H. Zhang, and M. Xian. Biosynthesis of natural rubber: Current state and perspectives. International Journal of Molecular Sciences, 20:50, 2018. doi: 10.3390/ijms20010050.

[17] J.E. Puskas, K. Chiang, and B. Barkakaty. Natural rubber (NR) biosynthesis: perspectives from polymer chemistry. In Chemistry, Manufacture and Applications of Natural Rubber, pages 30 – 67. Woodhead Publishing, 2014. ISBN 978-0-85709-683-8. doi: https://doi.org/10.1533/9780857096913.1.30.

[18] K.P. Menard and N.R. Menard. Dynamic Mechanical Analysis in the Analysis of Polymers and Rubbers, pages 1–33. American Cancer Society, 2015. ISBN 9780471440260. doi: 10.1002/0471440264.pst102.pub2.

[19] G. B. Ouyang. Network junction model for mechanical properties of filled vulcanizates. In Constitutive Models for Rubber III: Proceedings of the Third European Conference on Constitutive Models for Rubber, London, UK, 15-17 September 2003, pages 325–332. Taylor & Francis, 2003. ISBN 9789058095664.

[20] M. Klüppel. The role of disorder in filler reinforcement of elastomers on various length scales. In Filler-Reinforced Elastomers/Scanning Force Microscopy, pages 1–86. Springer Berlin Heidelberg, 2003. doi: 10.1007/b11054.

[21] S. Cantournet, R. Desmorat, and J. Besson. Mullins effect and cyclic stress softening of filled elastomers by internal sliding and friction thermodynamics model. International Journal of Solids and Structures, 46(11-12):2255–2264, 2009. doi: 10.1016/j.ijsolstr.2008.12.025.

[22] R. Raghunath, D. Juhre, and M. Klüppel. A physically motivated model for filled elastomers including strain rate and amplitude dependency in finite viscoelasticity. International Journal of Plasticity, 78:223–241, 2016. doi: 10.1016/j.ijplas.2015.11.005.

[23] M. Sobera and J. Hetper. Pyrolysis–gas chromatography–mass spectrometry of cured phenolic resins. Journal of Chromatography A, 993(1):131 – 135, 2003. ISSN 0021-9673. doi: https://doi.org/10.1016/S0021-9673(03)00388-1.

[24] C. Zhang, W.K. Binienda, L. Zeng, X. Ye, and S. Chen. Kinetic study of the novolac resin curing process using model fitting and model-free methods. Thermochimica Acta, 523(1):63 – 69, 2011. ISSN 0040-6031. doi: https://doi.org/10.1016/j.tca.2011.04.033.

[25] H. Dressler. Resorcinol: Its Uses and Derivatives. Springer US, 1994. doi: 10.1007/978-1-4899-0999-2.

[26] R.B. Durairaj. Resorcinol: Chemistry, Technology and Applications. Springer-Verlag, 2005. doi: 10.1007/3-540-28090-1.

[27] B. Derakhshandeh, A. Shojaei, and M. Faghihi. Effects of rubber curing ingredients and phenolic-resin on mechanical, thermal, and morphological characteristics of rubber/phenolic-resin blends. Journal of Applied Polymer Science, 108(6):3808–3821, 2008. doi: 10.1002/app.28034.

[28] E. Leicht; R. Sattelmeyer. Phenolic resins for rubber reinforcement. Kautschuk und Gummi, Kunststoffe, 1987. ISSN 0022-9520.

[29] J. Nieberle, G. Paulus, H. Queins, and H. Schoeppl. Über die wirkung von phenol-formaldehyd-novokalen im kaustschuk. Kautschuk und Gummi, Kunststoffe, 1986. ISSN 0022-9520.

[30] U. Eisele. Introduction to Polymer Physics. Springer Berlin Heidelberg, 1990. ISBN 978-3-642-74434-1. doi: 10.1007/978-3-642-74434-1.

[31] J.D. Ferry. Viscoelastic Properties of Polymers. Wiley, 1980. ISBN 978-0-471-04894-7.

[32] M. Jain. Textbook Of Engineering Physics. Prentice-Hall Of India Pvt. Limited, 2009. ISBN 9788120338623.

[33] W. Bennett and A. Morrison. The Science of Musical Sound. Springer, Cham, 2018. ISBN 9783319927947. doi: 10.1007/978-3-319-92796-1.

[34] B. Balachandran and E.B. Magrab. Single Degree-of-Freedom Systems Subjected to Periodic Excitations, page 197–296. Cambridge University Press, 3 edition, 2018. doi: 10.1017/9781108615839.006.

[35] L. Schwab, N. Hojdis, J. Lacayo-Pineda, and M. Wilhelm. Fourier-transform rheology of unvulcanized, carbon black filled styrene butadiene rubber. Macromolecular Materials and Engineering, 301(4):457–468, 2016. doi: 10.1002/mame.201500356.

[36] T. Alfrey and P. Doty. The methods of specifying the properties of viscoelastic materials. Journal of Applied Physics, 16(11):700–713, 1945. doi: 10.1063/1.1707524.

[37] N. Vennemann, K. Bökamp, and D. Bröker. Crosslink density of peroxide cured TPV. Macromolecular Symposia, 245-246(1):641–650, 2006. doi: 10.1002/masy.200651391.

[38] N. Vennemann, C. Schwarze, and C. Kummerlöwe. Determination of crosslink density and network structure of NR vulcanizates by means of TSSR. Advanced Materials Research, 844: 482–485, 2013. doi: 10.4028/www.scientific.net/amr.844.482.

[39] A. Das, A. Sallat, F. Böhme, E. Sarlin, J. Vuorinen, N. Vennemann, G. Heinrich, and K. Stöckelhuber. Temperature scanning stress relaxation of an autonomous self-healing elastomer containing non-covalent reversible network junctions. Polymers, 10(1):94, 2018. doi: 10.3390/polym10010094.

[40] T. Chatterjee, N. Vennemann, and K. Naskar. Temperature scanning stress relaxation measurements: A unique perspective for evaluation of the thermomechanical behavior of shape memory polymer blends. Journal of Applied Polymer Science, 135(2):45680–45691, 2018. ISSN 1097-4628. doi: 10.1002/app.45680. 45680.

[41] J.H. Poynting. The wave motion of a revolving shaft, and a suggestion as to the angular momentum in a beam of circularly polarised light. Proceedings of the Royal Society of London. Series A, Containing Papers of a Mathematical and Physical Character, 82(557):560–567, 1909. doi: 10.1098/rspa.1909.0060.

[42] D.B. Williams and C.B. Carter. Transmission Electron Microscopy. Springer US, 2009. doi: 10.1007/978-0-387-76501-3.

[43] G.H. Michler. Electron Microscopy of Polymers. Springer Berlin Heidelberg, 2008. doi: 10.1007/978-3-540-36352-1.

[44] J. Heydenreich. Transmissions-elektronenmikroskopie (TEM). In Analytiker-Taschenbuch, pages 177–215. Springer Berlin Heidelberg, 1996. doi: 10.1007/978-3-642-60995-4_5.

[45] S.S. Sarkawi, W.K. Dierkes, and J.W.M. Noordermeer. Elucidation of filler-to-filler and filler-to-rubber interactions in silica-reinforced natural rubber by TEM network visualization. European Polymer Journal, 54:118–127, 2014. doi: 10.1016/j.eurpolymj.2014.02.015.

[46] D. Rugar and P. Hansma. Atomic force microscopy. Physics Today, 43(10):23–30, 1990. doi: 10.1063/1.881238.

[47] G. Haugstad. Atomic Force Microscopy. John Wiley & Sons, Inc., 2012. doi: 10.1002/9781118360668.

[48] Q. Zhong, D. Inniss, K. Kjoller, and V.B. Elings. Fractured polymer/silica fiber surface studied by tapping mode atomic force microscopy. Surface Science Letters, 290(1-2):L688–L692, 1993. doi: 10.1016/0167-2584(93)90906-y.

[49] B.V Derjaguin, V.M Muller, and Yu.P Toporov. Effect of contact deformations on the adhesion of particles. Journal of Colloid and Interface Science, 53(2):314–326, 1975. doi: 10.1016/0021-9797(75)90018-1.

[50] I.H. Syed, D. Klat, A. Braer, F Fleck, and J. Lacayo-Pineda. Characterizing the influence of reinforcing resin on the structure and the mechanical response of filled isoprene rubber. Soft Materials, 16(4):275–288, 2018. doi: 10.1080/1539445x.2018.1509872.

[51] I.H. Syed, P. Vouagner, F. Fleck, and J. Lacayo-Pineda. Nonlinearity in the mechanical response of rubber as investigated by high-frequency DMA. Polymers, 11(4):581, 2019. doi: 10.3390/polym11040581.

[52] I.H. Syed and J. Lacayo-Pineda. Superharmonic resonance in carbon-black-filled rubber by high-frequency DMA. Polymers, 11(10):1653, 2019. doi: 10.3390/polym11101653.